Am J Nucl Med Mol Imaging 2024;14(4):208-229
www.ajnmmi.us /ISSN:2160-8407/ajnmmi0157513

Review Article

Recent advances in imaging and artificial intelligence (AI) for quantitative assessment of multiple myeloma

Yongshun Liu[1*], Wenpeng Huang[1*], Yihan Yang[1], Weibo Cai[2], Zhaonan Sun[3]

[1]Department of Nuclear Medicine, Peking University First Hospital, Beijing 100034, China; [2]Department of Radiology and Medical Physics, University of Wisconsin-Madison, Madison, WI 53705, USA; [3]Department of Medical Imaging, Peking University First Hospital, Beijing 100034, China. [*]Equal contributors.

Received April 30, 2024; Accepted July 18, 2024; Epub August 15, 2024; Published August 30, 2024

Abstract: Multiple myeloma (MM) is a malignant blood disease, but there have been significant improvements in the prognosis due to advancements in quantitative assessment and targeted therapy in recent years. The quantitative assessment of MM bone marrow infiltration and prognosis prediction is influenced by imaging and artificial intelligence (AI) quantitative parameters. At present, the primary imaging methods include computed tomography (CT), magnetic resonance imaging (MRI), and positron emission tomography (PET). These methods are now crucial for diagnosing MM and evaluating myeloma cell infiltration, extramedullary disease, treatment effectiveness, and prognosis. Furthermore, the utilization of AI, specifically incorporating machine learning and radiomics, shows great potential in the field of diagnosing MM and distinguishing between MM and lytic metastases. This review discusses the advancements in imaging methods, including CT, MRI, and PET/CT, as well as AI for quantitatively assessing MM. We have summarized the key concepts, advantages, limitations, and diagnostic performance of each technology. Finally, we discussed the challenges related to clinical implementation and presented our views on advancing this field, with the aim of providing guidance for future research.

Keywords: Multiple myeloma, artificial intelligence, computed tomography, positron emission tomography, magnetic resonance imaging, quantitative evaluation, radiomics

Introduction

Multiple myeloma (MM) is a hematologic malignancy characterized by the terminal differentiation of monoclonal plasma cells, ranking second in prevalence among such disorders. The illness is characterized by the invasion of the bone marrow (BM) and the excessive production of abnormal monoclonal immunoglobulin, resulting in common symptoms such as high levels of calcium in the blood, kidney problems, low red blood cell count, and bone abnormalities (usually lytic lesions) [1]. And these performances serve as indicators for CRAB criteria [2]. MM has a range of disease stages, including monoclonal gammopathy of undetermined significance (MGUS), smoldering multiple myeloma (SMM), and MM [3, 4]. Typically, MM starts as a monoclonal gammopathy of undetermined significance (MGUS), affecting 3% to 5% of individuals over the age of 65. Around 20% of cases of MGUS will develop into MM or a similar condition within 25 years [5]. The prognosis for MM is generally poor. However, with the advent of immunotherapies such as anti-CD38 monoclonal antibodies [6] and targeted therapy using chimeric antigen receptor (CAR) T cells that target mature antigens on the surface of MM B cells [7], there has been a significant improvement in the prognosis for MM. In recent years, survival rates have seen marked increases [8]. However, current treatment methods cannot achieve a complete cure, with a 5-year survival rate of less than 60% [9]. Most patients eventually develop drug resistance and relapse [10].

The grading system at MM has undergone several changes. The Durie and Salmon staging system, created in 1975, considers hemoglobin and serum calcium levels, bone abnormalities, M-gradient, and kidney function. The primary goal of this system was to assess the extent of tumor presence and ascertain its influence on patients' response to treatment and their survival prospects. In Stage I, having only one osteolytic lesion on imaging was the criterion, whereas having multiple osteolytic lesions automatically classified a patient with MM as Stage III [11]. The use of this staging system has been widespread for around thirty years due to its significant predictive value and its consistency as a method for categorizing patients in clinical trials. The Durie & Salmon Plus staging system [12] in 2003, categorizes widespread illness by counting focal lesions using whole-body MRI or PET/CT scans. The severity of the stages varied, with IA indicating a solitary plasmacytoma, IB representing fewer than five focal lesions, II denoting 5-20 focal lesions, and III indicating more than 20 focal lesions. The disease has been categorized by the internationally recognized International Staging System (ISS) since 2005, using β2-microglobulin and albumin levels as criteria [13, 14]. ESMO has incorporated the updated revised ISS system, which now considers cytogenetics and lactate dehydrogenase levels to improve risk evaluation [13].

https://doi.org/10.62347/NLLV9295

Imaging plays a crucial role in diagnosing, predicting outcomes, evaluating treatment effectiveness, monitoring progress, and detecting potential recurrence of MM [15, 16] (**Table 1**). However, there are significant variations in image interpretation in conventional imaging, and the small lytic lesions highlighted in the images are susceptible to infection by bone degenerative lesions [17]. Therefore, utilizing semi-quantitative or quantitative parameters to assess MM is more precise and crucial for diagnosis and prognosis prediction. At present, the primary imaging methods include computed tomography (CT), magnetic resonance imaging (MRI), and positron emission tomography (PET). Imaging and artificial intelligence (AI) methods are now utilized for quantitative assessment in MM diagnosis, as well as for evaluating myeloma cell infiltration, extramedullary disease, treatment effectiveness, and predicting prognosis (**Figure 1**). This review discusses the advancements in imaging methods, including CT, MRI, and PET/CT, as well as AI for quantitatively assessing MM. We have summarized the key concepts, advantages, limitations, and diagnostic performance of each technology. Finally, we discussed the challenges related to clinical implementation and presented our views on advancing this field, with the aim of providing guidance for future research.

Importance of imaging and AI in the quantitative evaluation of MM

Imaging plays a vital role in diagnosing and predicting the prognosis of MM. Osteolytic bone lesions, a form of osseous end-organ damage, are prevalent and significantly impact the health outcomes of individuals with MM. Around 70% of individuals with MM show bone damage when diagnosed [1]. Imaging can also reveal the presence of osseous and extraosseous plasmacytomas, which are abnormal growths of plasma cells. Furthermore, imaging studies enable the quantitative evaluation of bone marrow (BM) infiltration in MM. For nearly four decades, the standard imaging assessment for individuals with potential MM has been the traditional skeletal survey (CSS) [18] or whole-body X-ray (WBXR) [19]. The traditional method of WBXR (bone scan) can only identify lytic lesions if 30% to 50% of the cortex has been eroded. At that point, individuals are already in danger of developing pathological fractures. As a result, more advanced imaging techniques have replaced WBXR [16]. Advanced imaging methods like WBLDCT, WB-MRI, and PET/CT with ^{18}F-FDG are increasingly being utilized in the treatment of patients with MM. The diagnostic criteria for MM were updated by the International Myeloma Working Group (IMWG) in 2014 to include the presence of multiple lytic lesions on imaging tests such as CT, WBLDCT, or PET/CT, in addition to at least one distinct bone marrow focal lesion larger than 5 mm on MRI. This criterion is considered indicative of MM-related bone disease, even if not visible on skeletal radiography [4]. Additionally, the treatment response criteria in 2016 suggested assessing deeper imaging response with PET/CT in patients who have achieved complete response [20]. The guidelines were implemented after compelling evidence demonstrated that the new imaging methods have a higher detection rate than skeletal surveys. Consequently, these advanced imaging methods have become a routine part of clinical practice [21].

The complexity of MM lesions and their various manifestations in imaging limit the accuracy of diagnosis. Thus, advanced diagnostic methods are needed to provide accurate and personalized treatment for patients with this disease. AI, including machine learning and radiomics, represents the most recent advancement in the field of MM diagnosis and treatment. It enhances the sensitivity of examinations, effectively distinguishes MM from soluble metastases, and improves examination efficiency. Nevertheless, there are inherent limitations in detecting and characterizing bone changes in multiple myeloma (MM), making it a challenging task. Imaging and AI each have their advantages and disadvantages (**Table 2**), and various technologies can be selected for the diagnosis and treatment of MM based on specific situations.

Computed tomography (CT)

MM imaging has seen significant progress in recent years, especially with the transition from traditional radiography to CT scans. A groundbreaking study conducted by Schreiman and his team [22] in 1985 showed that CT scans had higher detection rates than traditional WBXR. CT shows promising characteristics that could potentially lead to its substitution for traditional radiography as a screening method for lytic lesions in MM. CT is superior to MRI in identifying osteolytic bone lesions and provides a more accurate assessment of spinal stability in vertebral fractures. On the other hand, MRI is considered the most reliable technique for identifying BM infiltration before bone fracture and assessing various aspects of medullary involvement. However, due to various factors, there are significant discrepancies in the interpretation of CT images. Thus, the Myeloma Spine and Bone Damage Score (MSBDS) [23] was created to assess bone damage, fracture risk, and instability in MM in a quantitative manner. Its aim is to address the issue of variability and ensure reliable evaluation of CT data. The MSBDS criteria have proven to be efficient, reproducible, and easily integrated into daily clinical practice. It is crucial to emphasize that MSBDS is just one option for quantitatively assessing MM bone involvement and should be utilized as an initial step in accurately evaluating the patient's disability. A comprehensive evaluation using reliable and quantitative parameters is essential [24].

Whole-body low-dose computed tomography (WBLDCT)

WBLDCT has several advantages over traditional imaging modalities. It plays a crucial role in the management and treatment decisions for patients with MM [25], classifying

Table 1. Summary of studies using imaging to quantitatively assess multiple myeloma

Aim	Imaging	Cohort size	Findings	Reference
Comparation qualitative and quantitative CT and MRI parameters for longitudinal disease monitoring.	CT MRI	N = 31	Quantitative CT showed a significant increase in maximum bone attenuation ($P < 0.001$) and a significant decrease in minimum bone attenuation ($P < 0.002$). Quantitative MRI showed a significant reduction in signal intensity of STIR in the BM in patients with diffuse BM involvement reaching ($P < 0.001$).	Horger et al. [127]
Diagnosis of WBLDCT in detecting diffuse marrow infiltration.	WBLDCT	N = 76	Medullary attenuation differed significantly among mixed, nodular, and diffuse CT-based appendicular medullary cavity patterns in the femurs (mean, 34.23 HU and range, 15-61 HU; mean, 66.26 HU and range, 26-104 HU; mean, 92.80 HU and range, 53-127 HU, respectively).	Koutoulidis et al. [128]
Diagnosis and staging of patients with suspicion of MM.	WBLDCT	N = 138	In all 138 patients, image resolution was diagnostic, enabling correct classification of MM patients. WBLDCT showed a total of 328 pathologic bone findings in 81/138 patients.	Ippolito et al. [28]
Compares sensitivity and prognostic significance of WBCT and CSS in patients with SMM and MM.	WBLDCT	N = 212	Fifty-four of 212 patients (25.5%) had a negative CSS and a positive WBCT for osteolytic lesions ($P < 0.0001$). WBCT should be considered the current standard for the detection of osteolytic lesions in MM.	Hillengass et al. [29]
Detection of bone disease.	WBLDCT	N = 33	LDCT/PET sensitivity, specificity and accuracy were 89.4%, 98.3% and 93.5%.	Maggialetti et al. [129]
Identification of lesions in SMM patients with only bone disease progression.	WBLDCT	N = 100	A total of 31/100 patients (31%) progressed, but 10 patients (10%) were identified as progressives solely due to bone disease on WBLDCT.	Gavriatopoulou et al. [26]
Clinical significance of medullary abnormalities in the AS.	WBLDCT	N = 172	In SMM, the presence of abnormal medullary lesions was associated with increased incidence of high-risk cytogenetic abnormalities (34.4% vs. 7.7%; $P = 0.002$) and extramedullary disease (10.4% vs. 0%; $P = 0.032$). It was also an independent poor prognostic predictor (hazard ratio 3.546, $P = 0.04$).	Nishida et al. [35]
Management of patients with MM and precursor states.	WBLDCT	N = 116	WBLDCT led to a change in management in 32 patients (28%). In 65 patients (56%), WBCT was performed for surveillance of MM precursor disease or stable treated MM, and did not detect new lesions.	Simeone et al. [130]
An automatic bone segmentation in WBCT scans.	WBCT	N = 18	A dice score of 0.95 and an intersection over union of 0.91.	Klein et al. [124]
Assess the reliability of the myeloma spine and bone damage score (MSBDS).	WBCT	N = 15	ICC correlation coefficient was 0.87 (95% CI: 0.79-0.92), and the Cronbach's alpha was 0.93 (95% CI: 0.94-0.97).	Tagliafico et al. [23]
Detect BM infiltration and distinguish different patterns of BM infiltration.	DESCT	N = 50	AUC = 0.856 [95% CI, 81.4-89.1%] with sensitivity = 0.841 and specificity = 0.768, as well as between MM patients and control subjects (AUC = 0.910 [95% CI, 79.5-97.3%], sensitivity = 0.829 and specificity = 1.000).	Hu et al. [131]
Subjective and objective image quality comparison of bone microstructure and disease-related abnormalities.	DS-PCD-CT	N = 50	DS-PCD-CT significantly improves spatial resolution of bony microstructure and lytic bone lesions compared to DS-EID-CT.	Winkelmann et al. [132]
Evaluate VNCa images from dual-layer spectral CT (DLCT), correlating results with ADC values from MRI.	DLCT	N = 32	Measurements in VNCa-CT showed the highest correlation with ADC at CaSupp index 65.	Brandelik et al. [17]
Evaluate the ADCs in the BM and determine a threshold ADC that may help distinguish a diffuse from a normal pattern with high accuracy.	MRI	N = 99	ADCs of MRI in patients with MM differ significantly. A diffuse MRI pattern can be distinguished more objectively from a normal MRI pattern by adding quantitative diffusion-weighted imaging to standard MR imaging protocols.	Koutoulidis et al. [133]
Assessment of treatment response.	MRI	N = 64	The agreement between the DIET method and the clinical outcome reached 0.922 (59 of 64; $\kappa = 0.816$; AUC, 0.886 ± 0.042).	Zhou et al. [134]
Assess the potential usefulness of fat fraction (FF) and ADC in diagnosing and classifying MM patients according to BM infiltration patterns.	DWI	N = 43	ANOVA with Bonferroni's correction showed a significant difference in ADC values among the different groups of MM patients ($P < 0.05$), while FF was only significantly different between patients with diffuse infiltration and patients with FL ($P = 0.002$).	Berardo et al. [49]

Evaluate the value of the combined evaluation of SE MRI, DCE-MRI and DWI.	SE MRI, DCE-MRI, DWI	N = 27	The combined skeletal score could significantly differentiate between subgroups based on IMWG response criteria (P = 0.016). The gold standard plasmacytosis could significantly differentiate between subgroups based on MRI response criteria (P < 0.001), as well as slope (P < 0.001) and ADC (P = 0.006). There is a good agreement between IMWG and MRI response criteria (Kendall's coefficient = 0.761).	Dutoit et al. [50]
Evaluate DWI of the BM in the differentiation of MM.	DWI	N = 76	Spinal SE-MRI can differentiate among MM. DWI based on the SI on b1000 images and ADC values is increased in MM.	Dutoit et al. [51]
The feasibility of DWI for assessment of treatment response in myeloma.	DWI	N = 49	DWI scores were significantly different between observers (P < 0.001).	Giles et al. [52]
The influence of ADC on MM survival.	DWI	N = 381	In Cox proportional hazards model, the ADC value was considered to be an independent risk factor affecting PFS and OS of MM (both P < 0.001).	Zhang et al. [54]
The prognostic value of ADC.	DWI	N = 114	Mean ADC value of the representative background bone marrow predicts both PFS and OS.	Zhang et al. [55]
Evaluate treatment response.	WBMRI	N = 21	sFF (P < 0.0001) and ADC (P = 0.001) significantly increased in responders but not non-responders.	Latifoltojar et al. [56]
The quantification of tumor burden and the correlation between MRI and prognostic biomarkers.	WBMRI	N = 95	Quantitative WBMRI examination may serve as an effective complement to imaging diagnosis.	Sun et al. [57]
Qualitative and quantitative evaluations of diffuse infiltration patterns on MRI could identify HRMM.	WBMRI	N = 180	BMPCs as a significant independent risk factor for HRMM (odds ratio (OR) = 1.019, 95% CI 1.004-1.033), while FF was a significant independent protective factor associated with HRMM (OR = 0.972, 95% CI 0.946-0.999). The combination of BMPCs and FF achieved the highest AUC of 0.732, with sensitivity and specificity of 70.9% and 68.3%, respectively.	Sun et al. [58]
Assess the test-retest reproducibility and intra/interobserver ADC measurements of myeloma lesions using WB-DW-MRI at 3T MRI.	WBDWI	N = 47	Mean ADC measurements are repeatable and reproducible in focal lesions in multiple myeloma, while the ADC measurements of diffuse disease in MM are more subject to variation.	ElGendy et al. [135]
Assessment of bone involvement.	^{18}F-FDG PET/CT	N = 58	SUVmean [OR: 10.52 (95% CI, 5.68-19.48); P < 0.0001] and for the SDSUV [OR: 5.58 (95% CI, 3.31-9.42); P < 0.001] than for the SUVmax [OR: 1.01 (95% CI, 1.003-1.022); P = 0.003].	Takahashi et al. [136]
Prognostic value of ^{18}F-FDG PET/CT semi-quantitative parameter.	^{18}F-FDG PET/CT	N = 38	aMTV ≥ 90.97 cm^3, aTLG ≥ 283.31 g, hemoglobin (Hb) < 100 g/L, focal lesions (FLs) ≥ 10, percentage of circulating plasma cells (CPC%) ≥ 30%, creatinine (Cr) ≥ 177 umol/L, lactic dehydrogenase (LDH) ≥ 250 g/L might be the adverse prognostic factors of PFS in patients with NDMM, all P < 0.05.	Wan et al. [70]
Prediction of the OS with or without ASCT.	^{18}F-FDG PET/CT	N = 227	High SUVmax, SUVmean, MTV, TLG, and FL could predict worse OS (hazard ratio [HR] = 2.569, 2.649, 2.506, 2.839, and 1.988, respectively) in non-ASCT MM patients.	Lee et al. [71]
Prediction of PFS and OS using TLG and MTV.	^{18}F-FDG PET/CT	N = 192	Baseline TLG > 620 g and MTV > 210 cm^3 remained a significant factor of poor PFS and OS after adjusting for baseline myeloma variables.	McDonald et al. [73]
Prognosis prediction of MM patients using MTV and TLG.	^{18}F-FDG PET/CT	N = 185	High-burden MTV (≥ 56.4 cm^3), TLG (≥ 166.4 g) and high-risk PET/CT findings differed significantly in PFS and OS. High-burden MTV and TLG findings also predicted survival outcomes in young patients (age < 75 years) and patients with high-risk chromosomal abnormalities.	Terao et al. [74]
Quantitative evaluation of BM using ^{18}F-FDG uptake IBI.	^{18}F-FDG PET/CT	N = 59	IBI score is an objective measure of BM involvement in MM, allowing the categorization of patients in different degrees of aggressiveness of the bone disease.	Takahashi et al. [76]
Prognostic value of ^{18}F-FDG PET/CT in MM.	^{18}F-FDG PET/CT	N = 45	^{18}F-FDG-PET/CT before and shortly after allogeneic HCT is a powerful predictor for progression-free and OS in MM patients.	Stolzenburg et al. [137]
Prognosis prediction of MM.	^{18}F-FDG PET/CT	N = 48	SUVmax > 4.0, VB > 0.001, k3 > 0.038 and influx (Ki) > 0.015 in reference BM as well as SUVmax > 6.8 in myeloma lesions were associated with shorter PFS.	Sachpekidis et al. [138]

STIR, short tau inverted recovery sequence; MM, multiple myeloma; SMM, smoldering multiple myeloma; BM, bone marrow; OR, odds ratio; CI, confidence interval; IBI, intensity of bone involvement; OS, overall survival; PFS, progression-free survival; MTV, metabolic tumour volume; TLG, total lesion glycolysis; VNCa, virtual noncalcium; AUC, area under the curve.

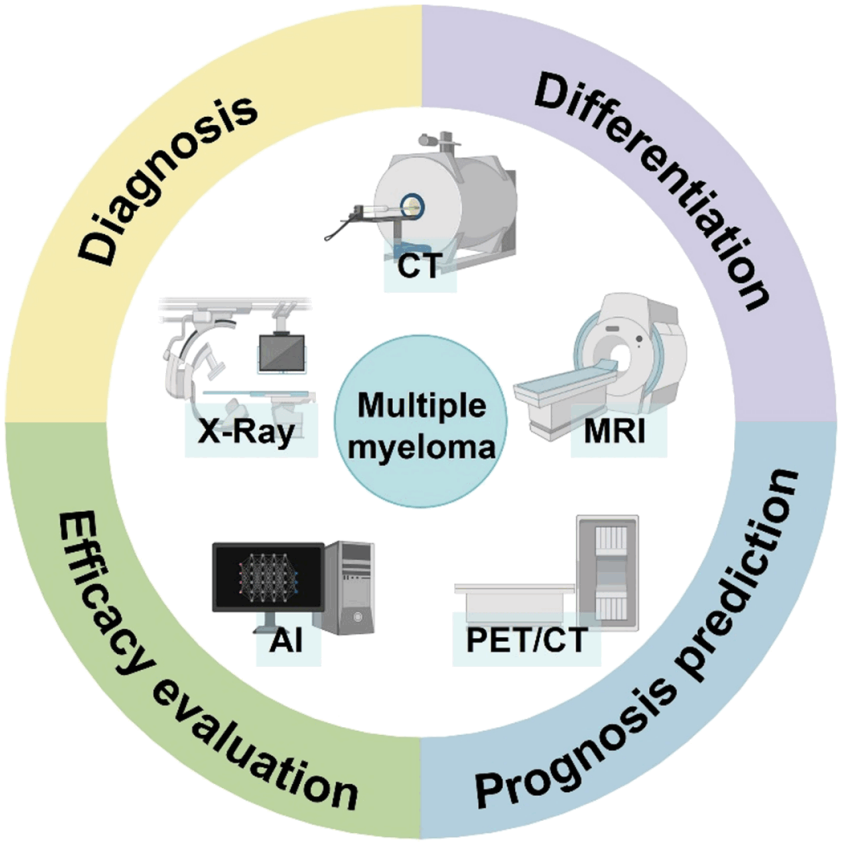

Figure 1. The applications of imaging techniques and artificial intelligence (AI) in quantitative evaluation of multiple myeloma (MM). Created with BioRender.com.

them based on disease progression, and implementing appropriate management strategies and treatment plans. For example, a study found that 10 of 100 patients only had WBLDCT diagnostic criteria and did not have CRAB criteria or defined events for myeloma [26]. Because early treatment can significantly improve the prognosis of MM, WBLDCT identification of early patients plays a crucial role in the management and treatment decisions of such patients. Additionally, WBLDCT has shown greater effectiveness than conventional plain radiography in evaluating the extent of MM involvement because it can detect both bone-destructive and extraosseous lesions. Horger et al. [27] emphasized the effectiveness of multidetector WBLDCT in assessing bone lesions associated with myeloma in their research study. The method demonstrated successful radiation, emphasizing the preservation of sensitivity and image clarity. Following their investigation, WBLDCT has become a common practice in European institutions for managing MM. Benefits of this technology include rapid scan times, clear images without the need for contrast agents, radiation levels similar to WBXR, and its utility in guiding biopsies and surgical procedures. WBLDCT has been developed for the purpose of identifying osteolytic lesions throughout the entire skeleton. With a high level of precision, this technology does not require contrast agents and reduces patient exposure to radiation by two to three times compared to traditional CT scans [28]. Multiple research studies have shown that WBLDCT is more effective than WBXR in detecting areas of bone loss. WBLDCT offers higher sensitivity and detection rates, particularly in the back and hip regions, leading to improved overall precision [29-33]. WBLDCT primarily identifies bone destruction but can also detect BM plasma cell (PC) infiltration in the long bones. The extent of BMPC infiltration in long bones tends to increase as the disease progresses. Furthermore, the prognosis of myeloma can vary depending on the infiltration pattern observed in the longitudinal BM.

Three patterns of abnormalities in the bone marrow of the appendicular skeleton, identified through WBLDCT, are classified as fatty, focal/scattered, and diffuse [34]. The fatty pattern is characterized by uniform low-density BM without any high-density lesions in the metaphysis and diaphysis. The focal pattern displays concentrated high-density spots, whereas the scattered pattern exhibits numerous dispersed areas of high density against a backdrop of low-density medullary BM in the appendicular skeleton. The scattered arrangement is characterized by a consistent high-density abnormality filling over 75.0% of the entire BM area in the metaphysis and diaphysis (**Figure 2A**). The diffuse pattern is associated with the poorest prognosis among these patterns, with the focal and fatty patterns following closely behind [34]. A study in 2017 by Hillengass et al. [29] compared the sensitivity and prognostic significance of WBLDCT and CSS, with the support of the IMWG, in detecting skeletal lesions. Additionally, they explored how the presence of additional lesions identified by WBLDCT relates to the prognosis for individuals with smoldering multiple myeloma (SMM) and MM. In the research, it was discovered that 25.5% of individuals exhibited a negative CSS but a positive WBLDCT for osteolytic lesions ($P < 0.0001$), suggesting that WBLDCT is now the preferred method for identifying osteolytic lesions in MM. Abnormal medullary lesions also play a significant role in predicting prognosis. Previous studies have shown that patients with SMM and abnormal medullary lesions have a lower overall survival (**Figure 2B**).

Skeletal surveys and WBLDCT are primarily used to detect osteolytic lesions, which can complicate the assessment of diffuse infiltrates and focal lesions in the trabecular bone's BM since they are not specifically examined. Moreover, the CSS method is time-consuming and requires patients to assume multiple positions. Performing WBXR is challenging due to the limited mobility caused by

Table 2. Advantages and limitations of imaging and artificial intelligence in multiple myeloma

Techniques		Advantages		Limitations
WBXR		Can identify lytic bone lesions.		Low detection rates may lead to potential delays in diagnosis and treatment. Inconvenient for elderly patients.
CSS		Evaluation of bone structures.		Bone lesion detection is easily interfered with, time-consuming, and requires frequent changes in body position.
CT	WBLDCT	Higher detection rates than WBXR. Compared to MRI, CT scans are more sensitive in evaluating osteolytic bone lesions. Supine position and short acquisition time.	Evaluate both osteolytic and extramedullary lesions. High accuracy, no need for contrast agents, and low radiation dose. Detection of plasma cell infiltration in the long bones' BM.	Evaluating diffuse infiltrates and focal lesions within the BM of the trabecular bone can be challenging.
	DECT		DECT with calcium-subtracted attenuation maps allows for quantifying BM infiltration levels.	The distribution of myeloma-associated plasma cells in bone is challenging to accurately assess because of its heterogeneous nature.
MRI	DWI	Standard method to detect BM infiltration; Higher sensitivity to invasive diseases compared to standard CT.	High significance lies in the qualitative evaluation of lesions, the high reliability of diagnosing focal lesions, and the improved definition of diffuse MRI patterns.	Limited imaging range, low specificity, extended duration, exorbitant cost, and contraindicated for patients with metallic implants.
	WBMRI		Fat quantification potential is valuable for detecting lesions and assessing response.	
	DCE-MRI		Evaluating a large amount of BM while reducing sampling bias from trephine biopsies is essential.	
PET/CT	^{18}F-FDG-PET/CT	Distinguish between active and inactive disease. Analysis in PET/CT images quantifies metabolic activity, providing a comprehensive evaluation of BM intensity.		False-negative and false-positive results. High blood sugar or recent use of high-dose steroids may result in false negatives.
AI		Efficient and quantitative. The differentiation between MM and lytic metastases.		Further research is needed to determine the diagnostic for MM; Data mutability is a significant issue; Lack of interoperable and standardized data analysis systems, the performance of AI models requires enhancement.

WBXR, whole-body X-ray; CSS, conventional skeletal survey; WBLDCT, whole body low-dose computed tomography; DECT, dual energy CT; MRI, magnetic resonance imaging; DWI, diffusion-weighted imaging; DCE, dynamic contrast-enhanced; PET, positron-emission tomography; AI, artificial intelligence; BM, bone marrow.

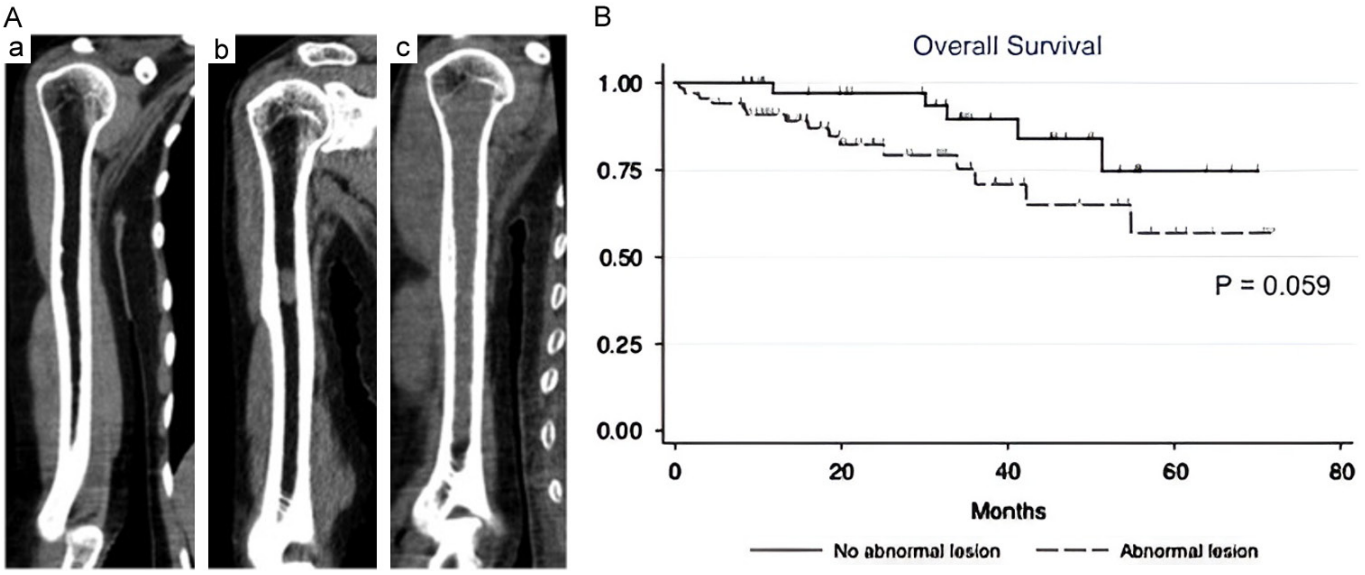

Figure 2. Prediction of cancer spread in bones of the limbs using WBLDCT. (A) Abnormalities in the appendicular skeleton in WBLDCT are categorized as: (a) fatty pattern, (b) focal pattern, and (c) diffuse pattern. Reproduced from ref [34], with permission from Elsevier, copyright 2018. (B) OS of symptomatic MM patients with or without abnormal medullary lesions. Reproduced from ref [35], with permission from Nature Publishing Group, copyright 2015. BM, bone marrow; OS, overall survival.

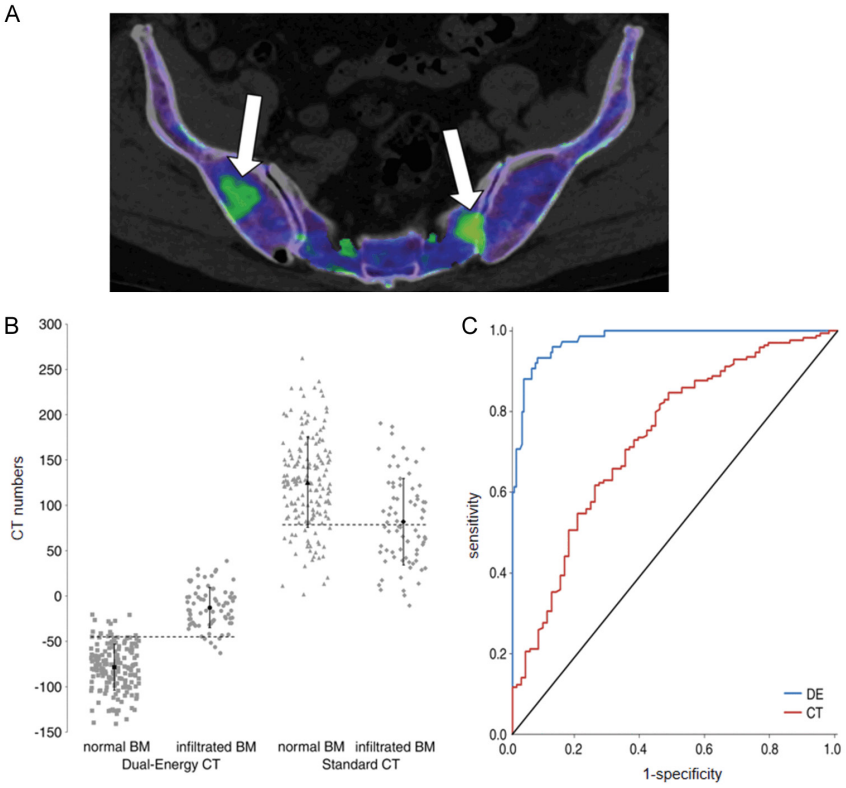

Figure 3. Anticipating the presence of BM infiltration using dual-energy VNCa images. A. The cross-sectional image of the pelvic region in an individual with progressing serologic myeloma. The DECT image with color-coding reveals two distinct lesions (indicated by arrows) highlighted in green, surrounded by normal marrow in blue. B. Scatterplots display the average CT values obtained from dual-energy VNCa images and weighted-average standard CT images for both infiltrated and normal bone marrow. A significant increase in CT values ($P < 0.001$) is observed on dual-energy VNCa images for infiltrated BM. C. ROC curves are used to distinguish between infiltrated and normal BM. The AUC using DE values obtained from VNCa images is 0.978. The AUC using standard CT numbers is 0.734. Reproduced from ref [38], with permission from Elsevier, copyright 2018. VNCa, virtual non-calcium; BM, bone marrow; AUC, area under the curve; ROC, receiver operating characteristic.

pain or fragility, especially in elderly individuals with myeloma. On the other hand, WBLDCT provides a more convenient option for these individuals. It is performed while lying down and has a quicker scanning time. Consequently, the 2019 IMWG imaging guidelines currently recommend WBCT as the initial diagnostic test for suspected myeloma [25].

Dual-energy CT (DECT)

DECT provides important information about the physical characteristics of tissues and can differentiate between tissues with similar absorption rates in traditional single-energy imaging [36] (**Figure 3A**). Although the IMWG guidelines do not currently endorse the use of CT attenuation assessment for diagnosis, DECT with the creation of calcium-subtracted attenuation maps offers an opportunity to measure the extent of BM infiltration. Prior research [37-42] on myeloma patients using DECT has mainly focused on identifying specific areas of concern in bone lesions that are correlated with MRI, as well as particular vertebrae or regions in the pelvis. Research has shown a correlation between the level of plasma cell infiltration in the bone marrow and the calcium-subtracted attenuation of the entire skeleton (**Figure 3B**, **3C**). An objective measure of marrow involvement is provided, potentially aiding in the early detection of the disease.

It is crucial to recognize that DECT analysis may not completely capture the varied distribution of plasma cells in the bone, as it focuses on a specific area rather than the entire bone. Currently, MRI is considered more effective than CT in assessing BM infiltration in MM, especially for infiltrative conditions. This has been highlighted in various studies [40]. DECT serves as an alternative for patients who are unable to undergo whole-body MRI.

Magnetic resonance imaging (MRI)

The IMWG now recognizes MRI as a key tool in diagnosing MM, alongside other indicators such as bone marrow plasma cells and serum-free light chain ratio. For patients with SMM at risk of progressing to MM, multiple focal lesions on MRI are necessary for a definitive diagnosis [43, 44]. MRI analyzes tissue composition without radiation, accurately detecting bone marrow invasion by myeloma cells. DWI and ADC measurements help differentiate tissues based on water and fat levels, with certain conditions exhibiting strong signals on imaging. Healthy individuals or those on certain medications may have different MRI results compared to those with normal BM. MRI typically shows MM lesions as having a lower signal in T1-weighted images and a higher signal in T2-weighted images. These lesions also exhibit fat suppression in opposed-phase imaging and increased contrast in T1-weighted sequences [43]. To assess the signal strength of a focal lesion, the intervertebral disc is often used as a reference, with a minimum diameter of 5 mm used to define the lesion. MM has five distinct MRI patterns for marrow involvement: normal, focal, diffuse, combined focal and diffuse, and 'salt and pepper' [45, 46] (**Figure 4A**). The infiltration patterns of BM have predictive significance in newly diagnosed MM. The presence of more than seven focal lesions and homogeneous diffuse infiltration has been associated with a negative impact on survival [47]. However, the diffuse pattern can sometimes be challenging to interpret due to varying imaging features depending on the extent of infiltration. Therefore, DWI could be beneficial in that aspect.

Diffusion-weighted imaging (DWI)

DWI is an advanced MRI technique that analyzes the diffusion of water molecules in tissue [48]. It identifies regions of high cell density (restricted movement) in contrast to low cell density and/or enhanced microcirculation (increased movement) without the requirement of a contrast agent. Semi-quantitative parameters, such as the apparent diffusion coefficient (ADC), are used to assess the level of cellularity. Previous studies [49-55] have found significant differences in ADC values between myeloma-invaded bone marrow and healthy marrow, indicating that ADC can also be used as a prognostic indicator for patients (**Figure 4B**, **4C**).

DWI emerges as a robust technique with promising potential for assessing MM patients. Firstly, DWI enhances lesion visibility through qualitative evaluation and can further improve diagnostic certainty for focal lesions by utilizing ADC measurements. Furthermore, DWI can help provide a more accurate depiction of the widespread MRI pattern observed in MM. However, the scattered arrangement, as opposed to the concentrated arrangement, has not been included in the revised guidelines for identifying symptomatic myeloma [43].

Whole body MRI (WBMRI)

Recent advancements in radiofrequency (RF) technology have led to the integration of WBMRI into clinical practice. This achievement has been made possible through the utilization of high-density phased array coils that cover extensive anatomical regions, ensuring a satisfactory signal-to-noise ratio [43]. WBDWI, a diffusion-weighted imaging called DWIBS, enables a comprehensive qualitative evaluation of disease burden in MM by identifying areas of high signal intensity on high b-value images. Quantitative studies [56-58] involving WBDWI often include calculating the total disease burden and analyzing the ADC of the bone marrow throughout the entire skeleton using segmentation methods to monitor treatment response [59]. Additionally, Dixon sequences, which rapidly generate four different images (in-phase, opposed phase, fat only, water only), are increasingly being incorporated into WBMRI protocols for MM. These sequences hold great potential for both lesion detection and response assessment, particularly due to their ability for fat quantification [60, 61].

Dynamic contrast-enhanced (DCE)-MRI

DCE-MRI has been used to assess perfusion in various anatomical regions, including the BM [43]. Typically, this procedure involves obtaining T1-weighted images dynamically before, during, and after injecting a paramagnetic contrast agent. The variations in signal strength in each pixel within the region under examination provide tissue-specific details related to vascular health. The most basic method, which does not involve numerical measurements, is to visually examine the shapes of the time-signal intensity curves (TICs) and categorize them into predetermined tissue-specific categories [62]. Evaluating a significant amount of bone marrow surpasses the sampling bias of trephine biopsies, offering a distinct advantage. The potential of DCE-MRI as a valuable clinical tool for treating plasma cell tumor patients is still uncertain, especially with the increasing popularity of DWI and WBDWI. Both DWI and WBDWI are non-invasive and safe alternatives that do not require intravenous contrast agents. MRI, including DWI, WBMRI, and DCE-MRI, has been increasingly used in patients with plasma cell neoplasms. Increasing evidence (**Table 1**) suggests that additional functional details related to tumor cellularity and angiogenesis could assist in diagnosing marrow infiltration and potentially predicting outcomes for patients with SMM and MM. Nevertheless, MRI has drawbacks such as

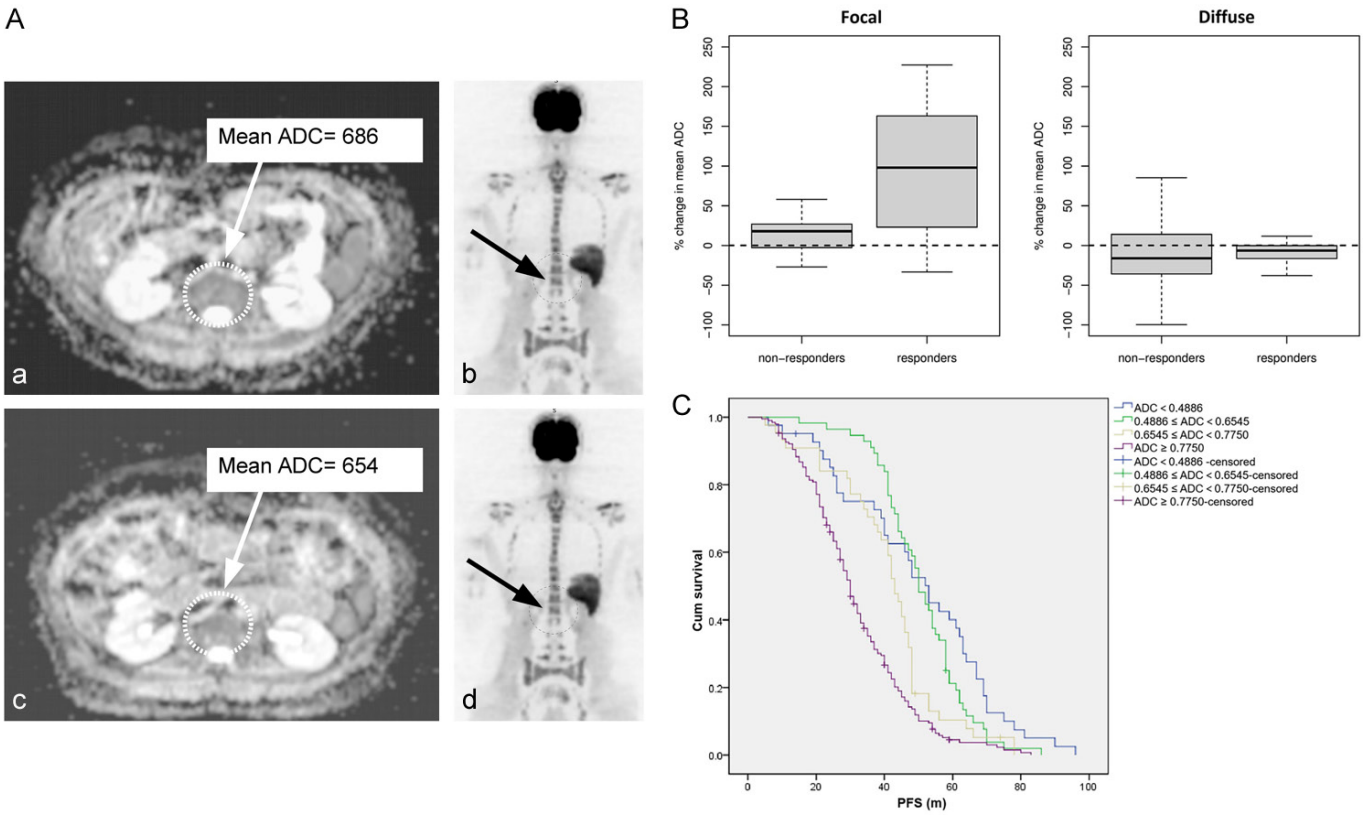

Figure 4. The ADC value of DWI predicts BM infiltration and prognosis. A. The diffuse salt-and-pepper pattern on axial DWI of the sacrum. a. Pre-treatment axial ADC map. b. Pre-treatment coronal inverted DWI. c. Post-treatment axial ADC map. d. Post-treatment coronal inverted DWI. The arrows point to the identical scattered lesion pattern in every image, along with the average ADC value displayed on the ADC maps. B. Boxplot illustrates the difference in the distribution of ΔADC percentage between responders and non-responders based on focal and diffuse patterns. The findings showed a significant increase in ADC among individuals who responded to treatment for specific lesions (odds ratio = 16.2, 95% CI: 3.87-67.4, $P = 0.0001$). Reproduced from ref [53], with permission from Elsevier, copyright 2017. C. Comparison of OS in patients with different ADC values. The unit of ADC value is 10^{-3} mm^2/s. Reproduced from ref [54], with permssion from Frontiers Media SA, copyright 2022. ADC, apparent diffusion coefficient; OS, overall survival.

extended scan duration, expensive price, restrictions for individuals with metal implants, challenges in imaging patients with claustrophobia, and limited scan coverage.

Positron-emission tomography/computed tomography (PET/CT)

PET/CT is a diagnostic procedure that uses radiolabeled ^{18}F-FDG to enable a comprehensive assessment of tumor morphology and functionality [63]. It has reported sensitivity and specificity in detecting bone lesions ranging between 80% and 100% [64, 65]. By combining CT imaging with ^{18}F-FDG, this method provides valuable information on hematologic malignancies such as myeloma [47] and lymphoma [66], as well as other types of cancer. PET/CT has a significant benefit in distinguishing between active and inactive diseases, which is essential for imaging purposes. Moreover, the incorporation of LDCT in combination with FDG-PET improves the accuracy of detecting bone and extramedullary abnormalities, thereby enhancing its diagnostic precision [15]. Research comparing whole-body MRI and PET/CT has shown similar sensitivity in identifying focal lesions (FLs), with MRI being more sensitive but less specific in detecting lesions. However, PET/CT has shown an advantage in detecting treatment response earlier than MRI. Persistent lesions following treatment can be challenging to assess because successfully treated lesions may show increased signal intensity on certain imaging sequences [67, 68]. The importance of PET-positive lesions in predicting outcomes has been emphasized in multiple studies, both at the time of first diagnosis and during recurrence [69].

Studies employing numerical analysis have assessed the predictive value of FDG measurements in determining the overall survival (OS) or progression-free survival (PFS) in individuals diagnosed with multiple myeloma (MM). Metabolic tumor volume (MTV), total lesion glycolysis (TLG), and Intensity of Bone Involvement (IBI) are among the primary FDG parameters that are typically analyzed. MTV and TLG (**Figure 5A**) have been recognized as significant predictors of outcomes in untreated MM patients in real-world settings [70]. High levels of SUVmax, SUVmean, MTV, TLG, and FL in MM patients who do not receive autologous stem cell transplantation (ASCT) have been linked to poorer OS rates [71]. MTV and TLG have been proposed as potential metabolic measures for assessing

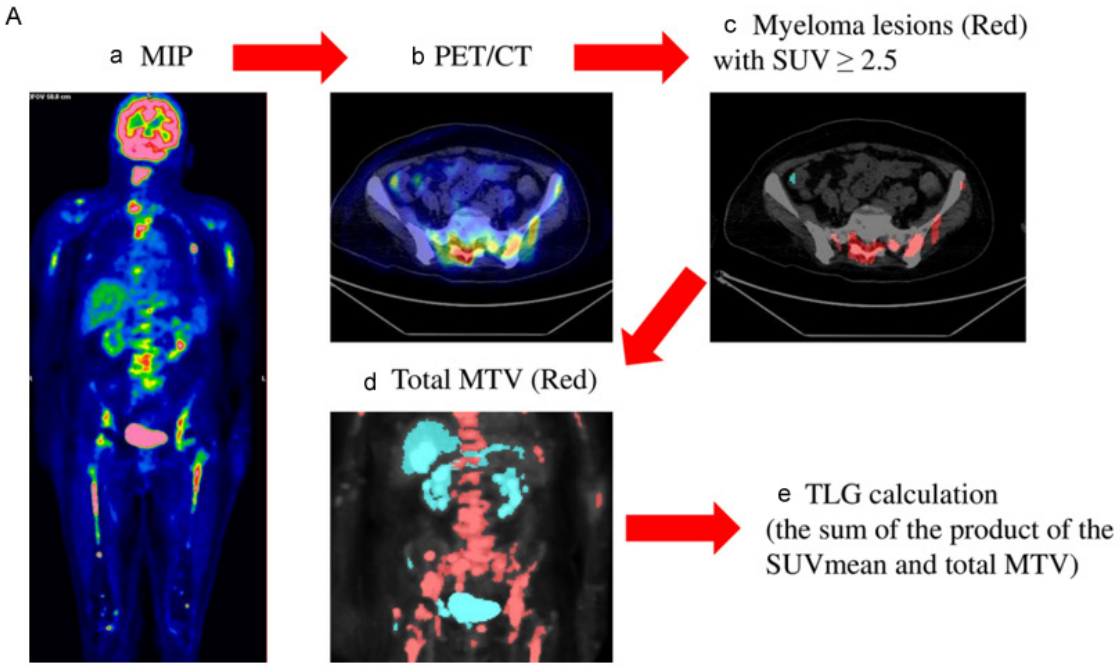
A
a MIP
b PET/CT
c Myeloma lesions (Red) with SUV ≥ 2.5
d Total MTV (Red)
e TLG calculation (the sum of the product of the SUVmean and total MTV)

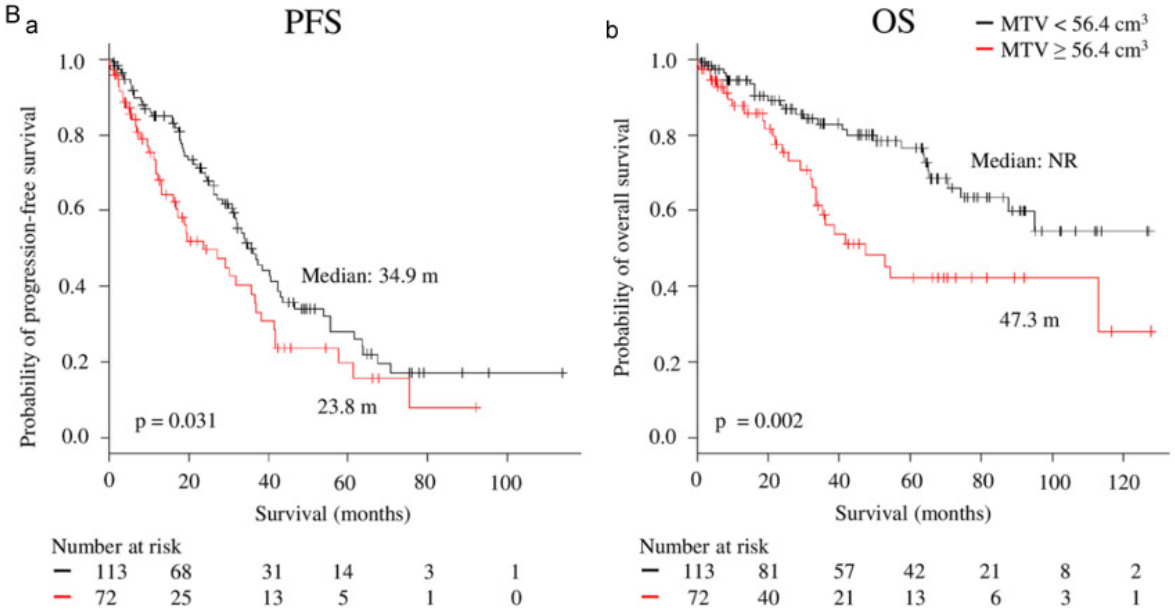
B
a
PFS
Probability of progression-free survival
Median: 34.9 m
23.8 m
p = 0.031
Survival (months)
Number at risk
113 68 31 14 3 1
72 25 13 5 1 0
b
OS
MTV < 56.4 cm³
MTV ≥ 56.4 cm³
Probability of overall survival
Median: NR
47.3 m
p = 0.002
Survival (months)
Number at risk
113 81 57 42 21 8 2
72 40 21 13 6 3 1

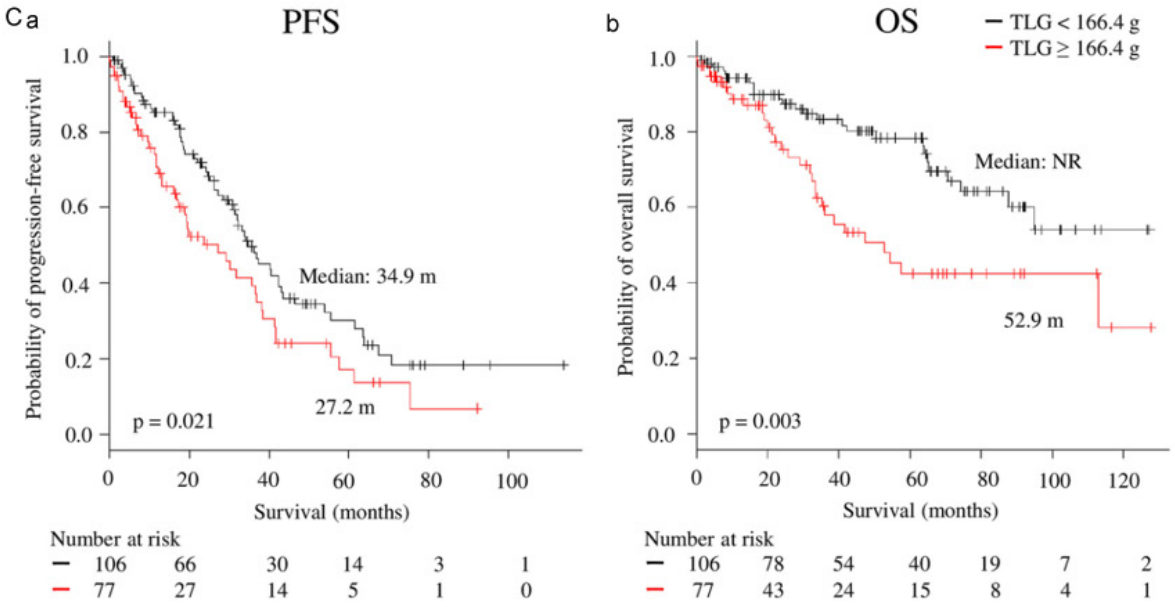
C
a
PFS
Probability of progression-free survival
Median: 34.9 m
27.2 m
p = 0.021
Survival (months)
Number at risk
106 66 30 14 3 1
77 27 14 5 1 0
b
OS
TLG < 166.4 g
TLG ≥ 166.4 g
Probability of overall survival
Median: NR
52.9 m
p = 0.003
Survival (months)
Number at risk
106 78 54 40 19 7 2
77 43 24 15 8 4 1

Figure 5. Prognosis prediction of MM patients by MTV and TLG. A. Calculating MTV and TLG from PET/CT images can be done in the following manner. a. The patient's MIP image shows numerous focal lesions. b, c. Lesions of interest were chosen and those with SUV ≥ 2.5 were highlighted in red. d. The sum of all red regions represents the total MTV. e. The TLG was determined by multiplying the SUVmean by the total MTV and summing the products. B. PFS and OS assessed by MTV using Kaplan-Meier estimation. C. PFS and OS assessed by TLG using Kaplan-Meier estimation. Reproduced from ref [74], with permission from Elsevier, copyright 2020. MIP, maximum intensity projection; PFS, progression-free survival; OS, overall survival; MTV, metabolic tumour volume; TLG, total lesion glycolysis.

tumor load and forecasting outcomes in MM [72-74] (**Figure 5B**, **5C**).

There are also studies that evaluate the relationship between other quantitative FDG parameters and the prognosis of MM. Takahashi et al. [75, 76] proposed a quantitative method for bone and BM evaluation using ^{18}F-FDG PET/CT, taking into account the extent and intensity of bone ^{18}F-FDG uptake, termed Intensity of Bone Involvement (IBI). IBI was defined by multiplying PBI by the mean Standardized Uptake Value (SUV) above hepatic uptake. They found that PET remission was related to ΔIBI < 0 (median = -0.10; -1.27 to +0.03), while PET progression was related to ΔIBI > 0 (median = 0.02; -0.07 to +0.29). They concluded that Delta IBI provides quantitative data for variations in ^{18}F-FDG uptake in the bone marrow during the follow-up of the patients. Higher IBI values at diagnosis are associated with an increased risk of patient mortality. In the diagnostic process and prognosis, PET/CT has numerous advantages. When it comes to evaluating bone (osteolytic) lesions in myeloma, WBLDCT and WBMRI are still the preferred choices. Nevertheless, experts from the American Roentgen Ray Society recommend PET/CT over axial MRI due to its ability to assess extramedullary solitary plasmacytomas when WBMRI is not accessible [77]. It is worth mentioning that ^{18}F-FDG-PET/CT is widely regarded as the preferred imaging technique for assessing and monitoring metabolic response to therapy [78]. Nevertheless, it is important to note that false-negative and false-positive results can occur with the use of FDG-PET/CT. Specifically, false-negative scans may be attributed to hyperglycemia or recent administration of high-dose steroids, which can lead to temporary metabolic suppression. Additionally, the wide availability of ^{18}F-FDG-PET/CT can be seen as a potential drawback.

Artificial intelligence (AI)

AI encompasses a range of tools and algorithms that aim to replicate human intelligence through computational means. AI in healthcare employs a variety of algorithms from machine learning and deep learning to automate tasks, leading to significant advancements. Machine learning and deep learning are closely associated with the radiomics process, which is a novel application of artificial intelligence in evaluating diseases for diagnosis, prognosis, and treatment assessment (**Table 3**). Radiomics relies on pattern recognition to extract quantitative descriptors from imaging data, typically acquired through structural modalities. These descriptors are then utilized in computational algorithms based on AI for predictive purposes [79-81]. AI is now being applied in the medical field not only for clinical studies, but also for clinical treatments of tumors [82-84]. Deep learning, a branch of machine learning, is influenced by the structure of the brain and utilizes artificial neural networks (ANN). It has emerged as the preferred method for automated image analysis [85]. Unsupervised machine learning involves no provided information, while supervised machine learning trains methods using existing data. Machine learning provides opportunities for creating analysis tools for CT, PET/CT, and MRI, which could improve or substitute existing evaluation techniques for these types of medical imaging [86].

Relevant research

Computerized tumor diagnosis is a critical aspect of medical AI applications. Several conventional machine learning methods, including random forests (RFs), k-nearest neighbors (kNNs), support vector machines (SVM), and artificial neural networks (ANNs), have been employed for the computational detection of MM. Nevertheless, specific constraints exist in the imaging assessment of MM that may affect the accuracy of the findings. Nevertheless, the integration of AI can enhance the sensitivity of individual imaging examinations. For instance, the interpretation of PET/CT scans may be affected by the varying patterns of BM infiltration, leading to reduced interobserver reproducibility. A new study introduced a state-of-the-art three-dimensional deep learning tool for automatically evaluating the level of BM metabolism in MM patients through PET/CT scans. The tool showcased the possibility of segmenting BM and computing MTV and TLG for all patients [87] (**Figure 6A**). Moreover, a strong positive relationship (P < 0.05) was found between the visual examination of PET/CT images and the values of MTV and TLG calculated using each of the six ^{18}F-FDG uptake thresholds. Identifying lithic bone lesions is essential for diagnosing, predicting outcomes, and choosing treatments for patients with MM [16]. Imaging techniques, including CT [88, 89], MRI [90, 91], ^{18}F-FDG PET [87, 92], and the utilization of a targeted PET tracer known as ^{68}Ga-Pentixafor [93], are utilized in machine learning or deep learning approaches for MM. These techniques are essential for determining the disease stage and evaluating therapy response.

Furthermore, recent advancements in deep learning have introduced various techniques such as multi-layer perceptron (MLP), recurrent neural networks (RNNs), and convolutional neural networks (CNNs). MLP is a type of neural network that organizes neurons into sequential layers, allowing information to flow in one direction. This

Table 3. Summary of studies using artificial intelligence to quantitatively assess multiple myeloma

Aim	Imaging	Cohort size	Findings	Reference
Machine learning or deep learning				
Segmentation effects of deep learning-based models on CT images for myeloma.	CT	N = 186	Deep learning is suggested in the segmentation and classification of CT images for myeloma, which can lift the detection accuracy.	Wang et al. [88]
Prognostic value of the sarcopenia.	CT	N = 322	Sarcopenia identified by a machine learning-based convolutional neural network algorithm significantly affects OS in patients with MM.	Nandakumar et al. [89]
The clinical utility of a phantom-based convolutional neural network noise reduction framework for WBLDCT skeletal surveys.	WBLDCT	N = 10	The phantom-based convolutional neural network noise reduction framework can improve visualization of critical structures within CT skeletal surveys.	Huber et al. [98]
Develop a deep learning algorithm and determine its performance at detecting lytic lesions.	WBLDCT	N = 40	Unet and "You Look Only Once" (YOLO) models were used as bone segmentation and lesion detection algorithms, detects lytic bone lesions of MM on WBLDCTs with high performance.	Faghani et al. [139]
Improve VNCa image quality for the assessment of focal MM, using an AGATE method.	DECT	N = 5	AGATE demonstrated reduced noise and artifacts in VNCa images and ability to improve visualization of BM lesions for assessing MM.	Gong et al. [140]
Validate a novel three-dimensional deep learning-based tool on PET/CT images for automated assessment of the intensity of BM metabolism in MM.	^{18}F-FDG PET/CT	N = 35	BM segmentation and calculation of MTV and TLG after the application of the deep learning tool were feasible. A significant positive correlation ($P < 0.05$) was observed between the results of the visual analysis of the PET/CT scans for the three patient groups and the MTV and TLG values after the employment of all six ^{18}F-FDG uptake thresholds.	Sachpekidis et al. [87]
Deep learning methods to automatically combine characteristics of PET and CT for whole-body MM bone lesion detection in a 3D manner.	^{68}Ga-Pentixafor PET/CT	N = 12	Deep learning method can leverage multimodal information for spatial feature representation, and W-Net obtained the best result for segmentation and lesion detection.	Xu et al. [93]
Establish an automated framework to predict local BM biopsy results from MRI.	MRI	N = 512	The automated image analysis framework allows for noninvasive prediction of a surrogate parameter for PCI, which is significantly correlated to the actual PCI from BM biopsy.	Wennmann et al. [99]
Differential diagnosis of MM, and different tumor metastasis lesions of the lumbar vertebra using machine learning.	MRI	N = 107	Machine learning-based classifiers showed a satisfactory performance in differentiating MM lesions from those of tumor metastasis.	Xiong et al. [90]
Discriminating MRD status in MM based on MRI and identify optimal machine learning methods to optimise the clinical treatment regimen.	MRI	N = 83	The linear SVM achieved the best performance compared to other classifiers, with AUCs of 0.811 and 0.708. The linear SVM-based machine learning method can offer a non-invasive tool for discriminating MRD status in MM.	Xiong et al. [91]
Use machine learning methods to explore OS-related prognostic factors.	/	N = 338	Deep learning can be used to predict OS in MM. C-indexes of 0.769, 0.780, 0.785, 0.798 and IBS score of 0.142, 0.112, 0.108, 0.099 were obtained from the CPH model, DeepSurv, DeepHit, and the RSF model.	Bao et al. [141]
Enhance the detection rate and execute an early and more precise disease management.	/	N = 4187	The model established by AI derived from routine laboratory results can accurately diagnose MM, which can boost the rate of early diagnosis.	Yan et al. [142]
Develop a computer-assisted method based on PET quantitative image features to assist diagnoses and treatment decisions for MM.	PET	N = 66	(VIMP + RSF) provides better results (C-index of 0.36) than conventional methods such as Lasso-Cox and gradient-boosting Cox (0.48 and 0.56).	Morvan et al. [143]
Radiomics analysis				
Using radiomics analysis to detect MM infiltration of the BM on CT scans of patients with osteopenia.	CT	N = 104	The AUC of the radiomics model was not significantly different from those of the radiologists ($P = 0.056$-0.821).	Park et al. [101]
Prediction in MM patients undergoing autologous transplantation.	CT	N = 84	AI-based interpretation of radiomics features stratified relapsed and non-relapsed MM patients.	Schenone et al. [102]
Prediction of OS in MM using MRI-based BM radiomics.	MRI	N = 121	The MRI-based BM radiomics may be useful for MM OS prediction. The radiomics signature, 1q21 gain, del (17p), and β2-MG ≥ 5.5 mg/L showed significant association with MM OS.	Li et al. [103]
Identify significant radiomics features based on MRI and establish effective models for predicting the response to bortezomib-based regimens.	MRI	N = 95	MRI-based radiomics had the potential to guide clinicians in MM management (AUC: 0.84-0.896 in the training set, 0.801-0.885 in the validation set).	Li et al. [104]

Establish a vertebral MRI-based radiomics model that could differentiate MM from metastases and compare the model performance with different features number.	MRI	N = 241	The AUCs of 20EPV-Model, 15EPV-Model, and CSF-Model (AUC = 0.71, 0.81, and 0.78) were poor than 10EPV-Model (AUC = 0.84, $P < 0.001$).	Liu et al. [105]
Investigate the feasibility of predicting HRCAs using a spinal MRI-based radiomics method.	MRI	N = 248	Comparable AUC values were observed between the radiomics model and the combined model in validation cohorts (AUC: 0.863 vs. 0.870, respectively, $P = 0.206$).	Liu et al. [106]
Develop and test an MRI-based radiomics model for predicting an HRC status in MM.	MRI	N = 89	Radiomics features based on two-sequence MRI showed good performance in differentiating HRC and non-HRC statuses in MM.	Liu et al. [107]
Implement a concept for automatic, comprehensive characterization of the BM from WBMRI.	MRI	N = 102	This pilot study demonstrates the feasibility of automatic, objective, comprehensive BM characterization from WBMRI in multicentric data sets.	Wennmann et al. [108]
Train and test an algorithm for automatic pelvic bm analysis from whole-body ADC maps in MM.	MRI	N = 54	U-Net was trained that can automatically segment pelvic bm from whole-body ADC maps in multicentric data sets with a quality comparable to manual segmentations.	Wennmann et al. [109]
Explore the clinical utility of spinal MRI-based radiomics to predict treatment response in MM.	MRI	N = 123	Nomograms incorporating MRI-based radiomic signature and ISS stage help predict the response to chemotherapy for MM.	Wu et al. [110]
Develop a radiomics nomogram based on MRI of the lumbar spine to detect MRD after MM treatment.	MRI	N = 130	The lumbar MRI-based radiomics nomogram can help detect MRD status in MM patients after treatment.	Wu et al. [111]
Develop an MRI-based radiomics nomogram for the differentiation of spinal metastasis and MM.	MRI	N = 312	The AUC values of the radiomics nomogram (0.853 and 0.762, respectively) were significantly higher than that of the clinical factor model (0.692 and 0.540, respectively) in both validation ($P = 0.048$) and external test ($P < 0.001$) sets.	Zhang et al. [112]
Develop a PET/CT radiomics-based model that could improve the diagnosis of multiple myeloma diffuse disease on ^{18}F-FDG PET/CT.	^{18}F-FDG PET/CT	N = 30	AUC of 0.90 (95% CI, 0.89-0.91). Radiomics analysis of ^{18}F-FDG PET/CT images with machine-learning overcame the limitations of visual analysis.	Mesguich et al. [92]
Identify spine MM using radiomics models.	^{18}F-FDG PET/CT	N = 131	Satisfactory performance of the three radiomics models was achieved in both the training and the validation groups (Training: AUC: CT: 0.909, PET: 0.949, ComModel: 0.973; Validation: AUC: CT: 0.897, PET: 0.929, ComModel: 0.948).	Jin et al. [113]
Prognostic value of radiomics features extracted from ^{18}F-FDG-PET/CT images and integrated with clinical characteristics and conventional PET/CT metrics.	^{18}F-FDG PET/CT	N = 98	AUC 0.761, sensitivity 56.7%, specificity 85.7%, $P < 0.05$ in training cohort and AUC 0.650, sensitivity 80.0%, specificity 78.6%, $P < 0.05$ in validation cohort. Radiomics features combined with clinical characteristic may provide clinical value for MM prognosis prediction.	Ni et al. [114]
Prognosis of MM using radiomics data.	^{18}F-FDG PET/CT	/	^{18}F-FDG PET/CT based radiomics models implemented with machine learning algorithms can improve the progress prediction.	Zhong et al. [115]

MM, multiple myeloma; BM, bone marrow; OR, odds ratio; CI, confidence interval; OS, overall survival; PFS, progression-free survival; MTV, metabolic tumour volume; TLG, total lesion glycolysis; VNCa, virtual noncalcium; AUC, area under the curve; MRD, minimal residual disease; SVM, support vector machine; HRCAs, high-risk cytogenetic abnormalities; AGATE, artificial intelligence based generalizable algorithm for multi-energy CT.

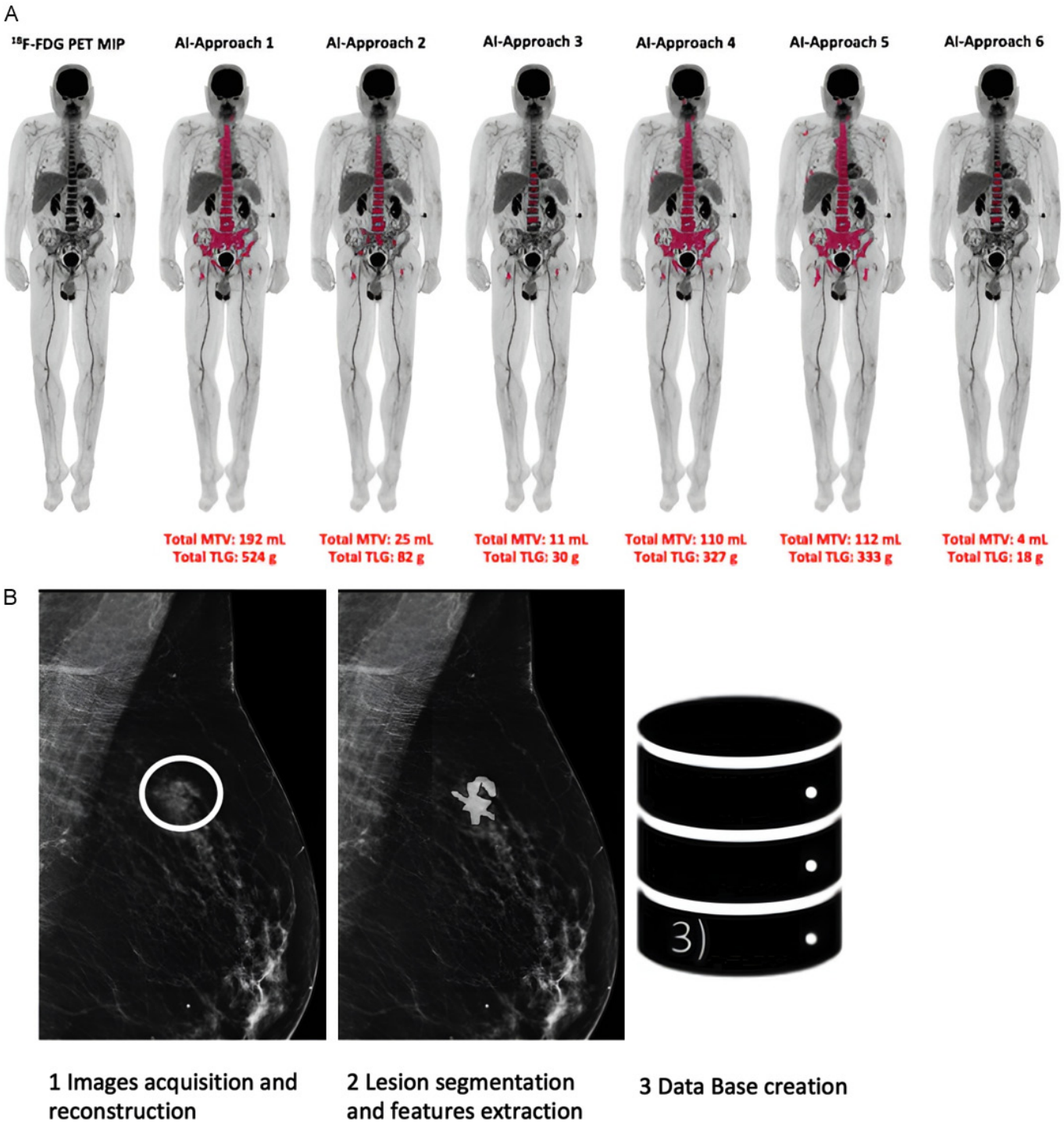

Figure 6. The application of AI in the calculation of MTV and TLG and the radiomics flowchart. A. An illustration of utilizing the AI-powered software tools to calculate the overall MTV and TLG showing significant widespread BM ^{18}F-FDG uptake. Reproduced from ref [87], with permission from Springer Nature, copyright 2023. B. Radiomics flowchart. The initial stage involved obtaining and reconstructing images. Following the adjustment of the image, the next stage involves segmenting and extracting features. Finally, data is organized and collected before analysis. Reproduced from ref [100], with permission from Elsevier, copyright 2020. MTV, metabolic tumour volume; TLG, total lesion glycolysis; BM, bone marrow.

architecture utilizes backpropagation to facilitate learning. However, MLPs are susceptible to overfitting, which can hinder their performance [94]. On the other hand, RNNs are particularly useful for studying sequential data, such as DNA sequences. CNNs can acquire invariant characteristics and detect spatial relationships in image data [95, 96]. They employ ranked hierarchies, where the distribution of inputs changes during the learning process [97]. In the field of MM research, the clinical feasibility of CNNs based on WBLDCT [98] and MRI [99] bone investigations was evaluated. These deep learning techniques have shown the potential to outperform traditional machine learning systems. Xu and colleagues [93] utilized deep learning techniques to automatically integrate fea-

tures from ^{68}Ga-Pentixafor PET/CT images for the detection of bone lesions in MM throughout the entire body in a three-dimensional manner. Lesion segmentation and detection were performed using two CNNs, namely V-Net and W-Net. The study indicated that the utilization of deep learning techniques can be highly advantageous in harnessing multimodal data for spatial feature representation, with W-Net surpassing traditional machine learning systems such as SVM, RF, and k-NN.

Another application of AI, radiomics, has shown promising prospects in diagnosing MM and distinguishing it from lytic metastases. Radiomics and machine learning methods can be utilized in MM patients to predict outcomes using various imaging techniques such as CT, MRI, and PET. Nearly half of the radiomics studies have utilized MRI. CT radiomics may detect changes in bone trabecular structure [101, 102], whereas MRI radiomics can provide information on the composition of bone marrow tissue [103-112]. Radiomics based on PET can analyze the activity of MM lesions and determine how they are affected by treatment [92, 113-115]. By combining various imaging data, radiomics provides a comprehensive view of MM lesions, enabling the detection of distinct patterns and features in bones affected by MM that can effectively differentiate them from lytic metastases. The AI-based radiomics process typically involves three steps (**Figure 6B**), and initial findings from this approach demonstrate that AI can identify image properties that are largely associated with disease progression. Radiomics characteristics provide a comprehensive, quantitative evaluation of tumor features, enhancing diagnostic accuracy and potentially uncovering new imaging markers for MM [116]. However, despite the utilization of advanced techniques, detecting and characterizing bone alterations in MM remains a challenging task. Hybrid imaging techniques are particularly prone to inaccuracies when identifying small lesions. The limited use of radiomics in MM is mainly due to the characteristics of the lesions. These lesions are scattered throughout the bone marrow, which poses a significant challenge in accurately segmenting the entire tumor burden. This is further complicated by the uneven distribution of lesions across the skeleton [117] and the spatial heterogeneity of associated mutations [118]. The technology that can automatically segment a large number of focal lesions and extensive diffuse infiltrations helps reduce labor and is more reliable.

Challenges and prospects

The application of artificial intelligence in MM imaging is still in its early stages, and most radiomics methods require segmentation of the structures to be analyzed, which is time-consuming. Its usability in clinical settings still needs to be demonstrated [119]. Furthermore, differences exist in the research approaches of radiomics, and challenges persist in reproducibility, data sharing, and standardization of radiomic features, hindering their integration into clinical practice. The primary costs involve enhancing the performance of AI models, bolstering the computing power of the technology infrastructure, and optimizing automatic bone marrow segmentation techniques, all of which demand substantial investment in manpower and resources. However, the benefits of clinical deployment of AI are substantial. AI can automatically detect all MM lesions within the body and aid radiologists in image interpretation, thereby saving time and minimizing the risk of errors. Additionally, it offers disease risk assessments and tailored treatment strategies [120]. Controversies persist in the realm of medical ethics concerning AI. To protect the rights of relevant individuals from infringement, AI systems must incorporate algorithmic procedures and advanced detection technologies [121]. Implementing AI requires educating healthcare professionals on relevant knowledge and providing them with necessary skills training, along with refining the associated measures [122].

Potential solutions for the future translation of radiomics research into clinical practice include methods such as atlas-based semi-automatic segmentation of DWI and the integration of deep learning applications with radiomics [109, 123, 124]. Moreover, combining radiomics with genomics, proteomics, and metabolomics data shows the potential in providing a comprehensive understanding of MM. This merging may reveal complex connections between imaging characteristics and the fundamental molecular processes that drive the progression of diseases.

Conclusion

MM is a complex plasma cell disease with varying characteristics that can be challenging to diagnose due to its progression from a pre-malignant stage. Advancements in treatment have improved patient outcomes, leading to updated diagnostic criteria by the IMWG in 2014. The identification of biomarkers that effectively predict patients at high risk of developing active disease, along with advancements in laboratory and imaging techniques, also drove the development. It is crucial to recognize that traditional imaging techniques often result in significant discrepancies in image analysis, particularly in identifying minor lytic lesions. These lesions, highlighted in the images, are susceptible to being mistaken for degenerative bone lesions. To address this issue, the utilization of semi-quantitative or quantitative parameters to assess MM has proven to be more accurate and essential for both diagnosis and prognosis prediction. Whole-body low-dose CT, whole-body MRI, and PET-CT are crucial imaging methods for accurately diagnosing multiple myeloma and assessing the disease's overall condition. AI shows great potential in MM diagnosis by distinguishing between MM and lytic metastases.

Several issues still need to be discussed. Firstly, DWI has the potential to contribute to a more precise characteriza-

tion of the diffuse MRI pattern in MM. The diffuse pattern, unlike the focal pattern, is not included in the revised diagnostic criteria for symptomatic myeloma. It may be worth considering including diffuse patterns in the most recent diagnostic criteria for symptomatic myeloma in the future. It is important to note that PET/CT is not the primary technique for evaluating bone (osteolytic) lesions in myeloma. It is crucial to consider methods to minimize the incidence of false-negative and false-positive results. Evaluation protocols for PET/CT and WB-MRI have been recently established by researchers; however, their prognostic value outside of clinical trials is still unknown. The lack of clarity could be attributed in part to the intricate management of multiple myeloma, which relies on the use of ASCT, the intensity and duration of therapy, and the susceptibility of the individual [125, 126]. Significant differences persist in the selection of imaging techniques for assessing individuals with multiple myeloma, accompanied by inconsistencies in image interpretation, which hinders reaching a consensus. As a result, the full potential of medical imaging in individuals with multiple myeloma has not been fully realized.

Traditional imaging has been applied in clinical practice for some time, and this technology is relatively mature. However, owing to technological limitations, there is still room for improvement in imaging accuracy. The future direction of traditional imaging may lie in its integration with AI. Future advancements and potential breakthroughs in AI for MM may be found in enhancing the reproducibility of radiomic features and advancing data sharing and standardization, such as interoperable and standardized MM patient data analysis systems and radiomic practice guidelines. Currently, the majority of radiomic methods require segmentation of the target structure, a process that is excessively time-consuming and a significant barrier to their clinical adoption. Automated precision segmentation technologies are crucial for clinical applications. Currently, neural networks like 'U-Net' and 'V-Net' can perform accurate and efficient automatic segmentation. The future development of such technologies will be a key driver for expanding the clinical application of AI in MM. The utilization of AI in nuclear medical imaging has consistently shown improvements thus far. In the coming years, the utilization of AI and radiomics in analyzing different bone lesions and the extensive adoption of quantitative methods for interpreting CT, MRI, and PET/CT scans will offer fresh perspectives in the field of medical imaging. AI is expected to significantly influence decision-making in the future by efficiently managing routine tasks, optimizing workflow, and allowing more time for patient care.

Disclosure of conflict of interest

Weibo Cai declares conflict of interest with the following corporations: Actithera, Inc., Rad Source Technologies, Inc., Portrai, Inc., rTR Technovation Corporation, and Four Health Global Pharmaceuticals, Inc.

Address correspondence to: Zhaonan Sun, Department of Medical Imaging, Peking University First Hospital, No. 8 Xishiku Street, Xicheng District, Beijing 100034, China. E-mail: zhaonan_sun@163.com; Weibo Cai, Department of Radiology and Medical Physics, University of Wisconsin-Madison, K6/562 Clinical Science Center, 600 Highland Avenue, Madison, WI 53705, USA. E-mail: wcai@uwhealth.org

References

[1] Cowan AJ, Green DJ, Kwok M, Lee S, Coffey DG, Holmberg LA, Tuazon S, Gopal AK and Libby EN. Diagnosis and management of multiple myeloma: a review. JAMA 2022; 327: 464-77.

[2] International Myeloma Working Group. Criteria for the classification of monoclonal gammopathies, multiple myeloma and related disorders: a report of the International Myeloma Working Group. Br J Haematol 2003; 121: 749-57.

[3] Kumar SK, Rajkumar V, Kyle RA, van Duin M, Sonneveld P, Mateos MV, Gay F and Anderson KC. Multiple myeloma. Nat Rev Dis Primers 2017; 3: 17046.

[4] Rajkumar SV, Dimopoulos MA, Palumbo A, Blade J, Merlini G, Mateos MV, Kumar S, Hillengass J, Kastritis E, Richardson P, Landgren O, Paiva B, Dispenzieri A, Weiss B, LeLeu X, Zweegman S, Lonial S, Rosinol L, Zamagni E, Jagannath S, Sezer O, Kristinsson SY, Caers J, Usmani SZ, Lahuerta JJ, Johnsen HE, Beksac M, Cavo M, Goldschmidt H, Terpos E, Kyle RA, Anderson KC, Durie BG and Miguel JF. International myeloma working group updated criteria for the diagnosis of multiple myeloma. Lancet Oncol 2014; 15: e538-48.

[5] Ormond Filho AG, Carneiro BC, Pastore D, Silva IP, Yamashita SR, Consolo FD, Hungria VTM, Sandes AF, Rizzatti EG and Nico MAC. Whole-body imaging of multiple myeloma: diagnostic criteria. Radiographics 2019; 39: 1077-97.

[6] Boussi LS, Avigan ZM and Rosenblatt J. Immunotherapy for the treatment of multiple myeloma. Front Immunol 2022; 13: 1027385.

[7] Raje N, Berdeja J, Lin Y, Siegel D, Jagannath S, Madduri D, Liedtke M, Rosenblatt J, Maus MV, Turka A, Lam LP, Morgan RA, Friedman K, Massaro M, Wang J, Russotti G, Yang Z, Campbell T, Hege K, Petrocca F, Quigley MT, Munshi N and Kochenderfer JN. Anti-BCMA CAR T-cell therapy bb2121 in relapsed or refractory multiple myeloma. N Engl J Med 2019; 380: 1726-37.

[8] Joseph NS, Kaufman JL, Dhodapkar MV, Hofmeister CC, Almaula DK, Heffner LT, Gupta VA, Boise LH, Lonial S and Nooka AK. Long-term follow-up results of lenalidomide, bortezomib, and dexamethasone induction therapy and risk-adapted maintenance approach in newly diagnosed multiple myeloma. J Clin Oncol 2020; 38: 1928-37.

[9] Costa LJ, Brill IK, Omel J, Godby K, Kumar SK and Brown EE. Recent trends in multiple myeloma incidence and survival by age, race, and ethnicity in the United States. Blood Adv 2017; 1: 282-7.

[10] Ria R and Vacca A. Bone marrow stromal cells-induced drug resistance in multiple myeloma. Int J Mol Sci 2020; 21: 613.

[11] Durie BG and Salmon SE. A clinical staging system for multiple myeloma. Correlation of measured myeloma cell mass with presenting clinical features, response to treatment, and survival. Cancer 1975; 36: 842-54.

[12] Durie BG, Kyle RA, Belch A, Bensinger W, Blade J, Boccadoro M, Child JA, Comenzo R, Djulbegovic B, Fantl D, Gahrton G, Harousseau JL, Hungria V, Joshua D, Ludwig H, Mehta J, Morales AR, Morgan G, Nouel A, Oken M, Powles R, Roodman D, San Miguel J, Shimizu K, Singhal S, Sirohi B, Sonneveld P, Tricot G and Van Ness B; Scientific Advisors of the International Myeloma Foundation. Myeloma management guidelines: a consensus report from the scientific advisors of the International Myeloma Foundation. Hematol J 2003; 4: 379-98.

[13] Moreau P, San Miguel J, Sonneveld P, Mateos MV, Zamagni E, Avet-Loiseau H, Hajek R, Dimopoulos MA, Ludwig H, Einsele H, Zweegman S, Facon T, Cavo M, Terpos E, Goldschmidt H, Attal M and Buske C; ESMO Guidelines Committee. Multiple myeloma: ESMO clinical practice guidelines for diagnosis, treatment and follow-up. Ann Oncol 2017; 28: iv52-iv61.

[14] Greipp PR, San Miguel J, Durie BG, Crowley JJ, Barlogie B, Bladé J, Boccadoro M, Child JA, Avet-Loiseau H, Kyle RA, Lahuerta JJ, Ludwig H, Morgan G, Powles R, Shimizu K, Shustik C, Sonneveld P, Tosi P, Turesson I and Westin J. International staging system for multiple myeloma. J Clin Oncol 2005; 23: 3412-20.

[15] Zamagni E, Tacchetti P and Cavo M. Imaging in multiple myeloma: how? When? Blood 2019; 133: 644-51.

[16] Baffour FI, Glazebrook KN, Kumar SK and Broski SM. Role of imaging in multiple myeloma. Am J Hematol 2020; 95: 966-77.

[17] Brandelik SC, Skornitzke S, Mokry T, Sauer S, Stiller W, Nattenmüller J, Kauczor HU, Weber TF and Do TD. Quantitative and qualitative assessment of plasma cell dyscrasias in dual-layer spectral CT. Eur Radiol 2021; 31: 7664-73.

[18] Mosebach J, Thierjung H, Schlemmer HP and Delorme S. Multiple myeloma guidelines and their recent updates: implications for imaging. Rofo 2019; 191: 998-1009.

[19] Durie BG. The role of anatomic and functional staging in myeloma: description of Durie/Salmon plus staging system. Eur J Cancer 2006; 42: 1539-43.

[20] Kumar S, Paiva B, Anderson KC, Durie B, Landgren O, Moreau P, Munshi N, Lonial S, Bladé J, Mateos MV, Dimopoulos M, Kastritis E, Boccadoro M, Orlowski R, Goldschmidt H, Spencer A, Hou J, Chng WJ, Usmani SZ, Zamagni E, Shimizu K, Jagannath S, Johnsen HE, Terpos E, Reiman A, Kyle RA, Sonneveld P, Richardson PG, McCarthy P, Ludwig H, Chen W, Cavo M, Harousseau JL, Lentzsch S, Hillengass J, Palumbo A, Orfao A, Rajkumar SV, Miguel JS and Avet-Loiseau H. International myeloma working group consensus criteria for response and minimal residual disease assessment in multiple myeloma. Lancet Oncol 2016; 17: e328-e346.

[21] Regelink JC, Minnema MC, Terpos E, Kamphuis MH, Raijmakers PG, Pieters-van den Bos IC, Heggelman BG, Nievelstein RJ, Otten RH, van Lammeren-Venema D, Zijlstra JM, Arens AI, de Rooy JW, Hoekstra OS, Raymakers R, Sonneveld P, Ostelo RW and Zweegman S. Comparison of modern and conventional imaging techniques in establishing multiple myeloma-related bone disease: a systematic review. Br J Haematol 2013; 162: 50-61.

[22] Schreiman JS, McLeod RA, Kyle RA and Beabout JW. Multiple myeloma: evaluation by CT. Radiology 1985; 154: 483-6.

[23] Tagliafico AS, Valle C, Bonaffini PA, Attieh A, Bauckneht M, Belgioia L, Bignotti B, Brunetti N, Bonsignore A, Capaccio E, De Giorgis S, Garlaschi A, Morbelli S, Rossi F, Torri L, Caprioli S, Tosto S, Cea M and Dominietto A. Myeloma spine and bone damage score (MSBDS) on whole-body computed tomography (WBCT): multiple reader agreement in a multicenter reliability study. Diagnostics (Basel) 2022; 12: 1894.

[24] Albano D, Bruno A, Bruno F, Calandri M, Caruso D, Clemente A, Coppolino P, Cozzi D, De Robertis R, Gentili F, Grazzini I, Jannone ML, Liguori C, Natella R, Pace G, Posa A, Scalise P, Accarino B, Bibbolino C, Barile A, Grassi R and Messina C; Young SIRM Working Group. Impact of coronavirus disease 2019 (COVID-19) emergency on Italian radiologists: a national survey. Eur Radiol 2020; 30: 6635-44.

[25] Hillengass J, Usmani S, Rajkumar SV, Durie BGM, Mateos MV, Lonial S, Joao C, Anderson KC, García-Sanz R, Riva E, Du J, van de Donk N, Berdeja JG, Terpos E, Zamagni E, Kyle RA, San Miguel J, Goldschmidt H, Giralt S, Kumar S, Raje N, Ludwig H, Ocio E, Schots R, Einsele H, Schjesvold F, Chen WM, Abildgaard N, Lipe BC, Dytfeld D, Wirk BM, Drake M, Cavo M, Lahuerta JJ and Lentzsch S. International myeloma working group consensus recommendations on imaging in monoclonal plasma cell disorders. Lancet Oncol 2019; 20: e302-e312.

[26] Gavriatopoulou M, Boultadaki A, Koutoulidis V, Ntanasis-Stathopoulos I, Bourgioti C, Malandrakis P, Fotiou D, Migkou M, Kanellias N, Eleutherakis-Papaiakovou E, Kastritis E, Terpos E, Dimopoulos MA and Moulopoulos LA. The role of low dose whole body CT in the detection of progression of patients with smoldering multiple myeloma. Blood Cancer J 2020; 10: 93.

[27] Horger M, Claussen CD, Bross-Bach U, Vonthein R, Trabold T, Heuschmid M and Pfannenberg C. Whole-body low-dose multidetector row-CT in the diagnosis of multiple myeloma: an alternative to conventional radiography. Eur J Radiol 2005; 54: 289-97.

[28] Ippolito D, Besostri V, Bonaffini PA, Rossini F, Di Lelio A and Sironi S. Diagnostic value of whole-body low-dose computed tomography (WBLDCT) in bone lesions detection in patients with multiple myeloma (MM). Eur J Radiol 2013; 82: 2322-7.

[29] Hillengass J, Moulopoulos LA, Delorme S, Koutoulidis V, Mosebach J, Hielscher T, Drake M, Rajkumar SV, Oestergaard B, Abildgaard N, Hinge M, Plesner T, Suehara Y, Matsue K, Withofs N, Caers J, Waage A, Goldschmidt H, Dimopoulos MA, Lentzsch S, Durie B and Terpos E. Whole-body computed tomography versus conventional skeletal survey in patients with multiple myeloma: a study of the International myeloma working group. Blood Cancer J 2017; 7: e599.

[30] Hinge M, Andersen KT, Lund T, Jørgensen HB, Holdgaard PC, Ormstrup TE, Østergaard LL and Plesner T. Baseline bone involvement in multiple myeloma - a prospective comparison of conventional X-ray, low-dose computed tomography, and 18flourodeoxyglucose positron emission tomography in previously untreated patients. Haematologica 2016; 101: e415-e418.

[31] Pianko MJ, Terpos E, Roodman GD, Divgi CR, Zweegman S, Hillengass J and Lentzsch S. Whole-body low-dose computed tomography and advanced imaging techniques for

multiple myeloma bone disease. Clin Cancer Res 2014; 20: 5888-97.
[32] Pierro A, Posa A, Astore C, Sciandra M, Tanzilli A, Petrosino A, Del Balso MS, Fraticelli V, Cilla S and Iezzi R. Whole-body low-dose multidetector-row CT in multiple myeloma: guidance in performing, observing, and interpreting the imaging findings. Life (Basel) 2021; 11: 1320.
[33] Siontis B, Kumar S, Dispenzieri A, Drake MT, Lacy MQ, Buadi F, Dingli D, Kapoor P, Gonsalves W, Gertz MA and Rajkumar SV. Positron emission tomography-computed tomography in the diagnostic evaluation of smoldering multiple myeloma: identification of patients needing therapy. Blood Cancer J 2015; 5: e364.
[34] Matsue K, Kobayashi H, Matsue Y, Abe Y, Narita K, Kitadate A and Takeuchi M. Prognostic significance of bone marrow abnormalities in the appendicular skeleton of patients with multiple myeloma. Blood Adv 2018; 2: 1032-9.
[35] Nishida Y, Matsue Y, Suehara Y, Fukumoto K, Fujisawa M, Takeuchi M, Ouchi E and Matsue K. Clinical and prognostic significance of bone marrow abnormalities in the appendicular skeleton detected by low-dose whole-body multidetector computed tomography in patients with multiple myeloma. Blood Cancer J 2015; 5: e329.
[36] Hamid S, Nasir MU, So A, Andrews G, Nicolaou S and Qamar SR. Clinical applications of dual-energy CT. Korean J Radiol 2021; 22: 970-82.
[37] Gu R, Amlani A, Haberland U, Hodson D, Streetly M, Antonelli M, Dregely I and Goh V; Myeloma Imaging Research Group at Guy's and St Thomas' Hospitals, London and King's College London. Correlation between whole skeleton dual energy CT calcium-subtracted attenuation and bone marrow infiltration in multiple myeloma. Eur J Radiol 2022; 149: 110223.
[38] Kosmala A, Weng AM, Heidemeier A, Krauss B, Knop S, Bley TA and Petritsch B. Multiple myeloma and dual-energy CT: diagnostic accuracy of virtual noncalcium technique for detection of bone marrow infiltration of the spine and pelvis. Radiology 2018; 286: 205-13.
[39] Kosmala A, Weng AM, Krauss B, Knop S, Bley TA and Petritsch B. Dual-energy CT of the bone marrow in multiple myeloma: diagnostic accuracy for quantitative differentiation of infiltration patterns. Eur Radiol 2018; 28: 5083-90.
[40] Reinert CP, Krieg E, Esser M, Nikolaou K, Bösmüller H and Horger M. Role of computed tomography texture analysis using dual-energy-based bone marrow imaging for multiple myeloma characterization: comparison with histology and established serologic parameters. Eur Radiol 2021; 31: 2357-67.
[41] Thomas C, Schabel C, Krauss B, Weisel K, Bongers M, Claussen CD and Horger M. Dual-energy CT: virtual calcium subtraction for assessment of bone marrow involvement of the spine in multiple myeloma. AJR Am J Roentgenol 2015; 204: W324-31.
[42] Werner S, Krauss B and Horger M. Dual-energy CT-based bone marrow imaging in multiple myeloma: assessment of focal lesions in relation to disease status and MRI findings. Acad Radiol 2022; 29: 245-54.
[43] Koutoulidis V, Papanikolaou N and Moulopoulos LA. Functional and molecular MRI of the bone marrow in multiple myeloma. Br J Radiol 2018; 91: 20170389.
[44] Kastritis E, Moulopoulos LA, Terpos E, Koutoulidis V and Dimopoulos MA. The prognostic importance of the presence of more than one focal lesion in spine MRI of patients with asymptomatic (smoldering) multiple myeloma. Leukemia 2014; 28: 2402-3.
[45] Vande Berg BC, Kirchgesner T, Acid S, Malghem J, Vekemans MC and Lecouvet FE. Diffuse vertebral marrow changes at MRI: multiple myeloma or normal? Skeletal Radiol 2022; 51: 89-99.
[46] Moulopoulos LA, Varma DG, Dimopoulos MA, Leeds NE, Kim EE, Johnston DA, Alexanian R and Libshitz HI. Multiple myeloma: spinal MR imaging in patients with untreated newly diagnosed disease. Radiology 1992; 185: 833-40.
[47] Terao T and Matsue K. Progress of modern imaging modalities in multiple myeloma. Int J Hematol 2022; 115: 778-89.
[48] Koh DM and Collins DJ. Diffusion-weighted MRI in the body: applications and challenges in oncology. AJR Am J Roentgenol 2007; 188: 1622-35.
[49] Berardo S, Sukhovei L, Andorno S, Carriero A and Stecco A. Quantitative bone marrow magnetic resonance imaging through apparent diffusion coefficient and fat fraction in multiple myeloma patients. Radiol Med 2021; 126: 445-52.
[50] Dutoit JC, Claus E, Offner F, Noens L, Delanghe J and Verstraete KL. Combined evaluation of conventional MRI, dynamic contrast-enhanced MRI and diffusion weighted imaging for response evaluation of patients with multiple myeloma. Eur J Radiol 2016; 85: 373-82.
[51] Dutoit JC, Vanderkerken MA, Anthonissen J, Dochy F and Verstraete KL. The diagnostic value of SE MRI and DWI of the spine in patients with monoclonal gammopathy of undetermined significance, smouldering myeloma and multiple myeloma. Eur Radiol 2014; 24: 2754-65.
[52] Giles SL, Messiou C, Collins DJ, Morgan VA, Simpkin CJ, West S, Davies FE, Morgan GJ and deSouza NM. Whole-body diffusion-weighted MR imaging for assessment of treatment response in myeloma. Radiology 2014; 271: 785-94.
[53] Lacognata C, Crimì F, Guolo A, Varin C, De March E, Vio S, Ponzoni A, Barilà G, Lico A, Branca A, De Biasi E, Gherlinzoni F, Scapin V, Bissoli E, Berno T and Zambello R. Diffusion-weighted whole-body MRI for evaluation of early response in multiple myeloma. Clin Radiol 2017; 72: 850-7.
[54] Zhang B, Bian B, Zhang Y, Zhang L, Zhang R and Wang J. The apparent diffusion coefficient of diffusion-weighted whole-body magnetic resonance imaging affects the survival of multiple myeloma independently. Front Oncol 2022; 12: 780078.
[55] Zhang L, Wang Q, Wu X, Zhao A, Feng J, Zhang H, Cao X, Li S, Cai H, Sun Z, Duan M, Zhu T, Zhang W, Jin Z, Zhou D, Xue H and Li J. Baseline bone marrow ADC value of diffusion-weighted MRI: a potential independent predictor for progression and death in patients with newly diagnosed multiple myeloma. Eur Radiol 2021; 31: 1843-52.
[56] Latifoltojar A, Hall-Craggs M, Bainbridge A, Rabin N, Popat R, Rismani A, D'Sa S, Dikaios N, Sokolska M, Antonelli M, Ourselin S, Yong K, Taylor SA, Halligan S and Punwani S. Whole-body MRI quantitative biomarkers are associated significantly with treatment response in patients with newly diagnosed symptomatic multiple myeloma following bortezomib induction. Eur Radiol 2017; 27: 5325-36.
[57] Sun M, Cheng J, Ren C, Zhang Y, Li Y, Li Y and Zhang S. Quantitative whole-body MR imaging for assessment of tumor burden in patients with multiple myeloma: correla-

tion with prognostic biomarkers. Quant Imaging Med Surg 2021; 11: 3767-80.
[58] Sun M, Wang L, Wang C, Ma J, Wang W, Lin L, Ren C, Zhang Y and Cheng J. Quantitative analysis of whole-body MRI for accessing the degree of diffuse infiltration patterns and identifying high risk cases of newly diagnosed multiple myeloma. J Magn Reson Imaging 2024; 59: 2035-2045.
[59] Giles SL, deSouza NM, Collins DJ, Morgan VA, West S, Davies FE, Morgan GJ and Messiou C. Assessing myeloma bone disease with whole-body diffusion-weighted imaging: comparison with x-ray skeletal survey by region and relationship with laboratory estimates of disease burden. Clin Radiol 2015; 70: 614-21.
[60] Bray TJP, Singh S, Latifoltojar A, Rajesparan K, Rahman F, Narayanan P, Naaseri S, Lopes A, Bainbridge A, Punwani S and Hall-Craggs MA. Diagnostic utility of whole body Dixon MRI in multiple myeloma: a multi-reader study. PLoS One 2017; 12: e0180562.
[61] Latifoltojar A, Hall-Craggs M, Rabin N, Popat R, Bainbridge A, Dikaios N, Sokolska M, Rismani A, D'Sa S, Punwani S and Yong K. Whole body magnetic resonance imaging in newly diagnosed multiple myeloma: early changes in lesional signal fat fraction predict disease response. Br J Haematol 2017; 176: 222-33.
[62] Dutoit JC, Vanderkerken MA and Verstraete KL. Value of whole body MRI and dynamic contrast enhanced MRI in the diagnosis, follow-up and evaluation of disease activity and extent in multiple myeloma. Eur J Radiol 2013; 82: 1444-52.
[63] Ishii S, Yamakuni R, Sugawara S, Hara J, Endo Y, Hotsumi H, Hiruta M, Kobiyama H, Yaginuma Y, Fukushima K and Ito H. Investigation of factors affecting CT attenuation and glucose metabolism of bone marrow as seen on PET/CT scans. Am J Nucl Med Mol Imaging 2024; 14: 22-30.
[64] Moreau P, Attal M, Caillot D, Macro M, Karlin L, Garderet L, Facon T, Benboubker L, Escoffre-Barbe M, Stoppa AM, Laribi K, Hulin C, Perrot A, Marit G, Eveillard JR, Caillon F, Bodet-Milin C, Pegourie B, Dorvaux V, Chaleteix C, Anderson K, Richardson P, Munshi NC, Avet-Loiseau H, Gaultier A, Nguyen JM, Dupas B, Frampas E and Kraeber-Bodere F. Prospective evaluation of magnetic resonance imaging and [(18)F]Fluorodeoxyglucose positron emission tomography-computed tomography at diagnosis and before maintenance therapy in symptomatic patients with multiple myeloma included in the IFM/DFCI 2009 trial: results of the IMAJEM study. J Clin Oncol 2017; 35: 2911-8.
[65] Zamagni E, Patriarca F, Nanni C, Zannetti B, Englaro E, Pezzi A, Tacchetti P, Buttignol S, Perrone G, Brioli A, Pantani L, Terragna C, Carobolante F, Baccarani M, Fanin R, Fanti S and Cavo M. Prognostic relevance of 18-F FDG PET/CT in newly diagnosed multiple myeloma patients treated with up-front autologous transplantation. Blood 2011; 118: 5989-95.
[66] Zhang X, Huang W, Qiu Y, Chen Z, Song L, Yang Q and Kang L. (18)F-FDG PET/CT in extranodal natural killer/T-cell lymphoma: a comprehensive evaluation method. Am J Nucl Med Mol Imaging 2023; 13: 245-58.
[67] Sachpekidis C, Mosebach J, Freitag MT, Wilhelm T, Mai EK, Goldschmidt H, Haberkorn U, Schlemmer HP, Delorme S and Dimitrakopoulou-Strauss A. Application of (18)F-FDG PET and diffusion weighted imaging (DWI) in multiple myeloma: comparison of functional imaging modalities. Am J Nucl Med Mol Imaging 2015; 5: 479-92.
[68] Derlin T, Peldschus K, Münster S, Bannas P, Herrmann J, Stübig T, Habermann CR, Adam G, Kröger N and Weber C. Comparative diagnostic performance of ^{18}F-FDG PET/CT versus whole-body MRI for determination of remission status in multiple myeloma after stem cell transplantation. Eur Radiol 2013; 23: 570-8.
[69] Usmani SZ, Mitchell A, Waheed S, Crowley J, Hoering A, Petty N, Brown T, Bartel T, Anaissie E, van Rhee F and Barlogie B. Prognostic implications of serial 18-fluoro-deoxyglucose emission tomography in multiple myeloma treated with total therapy 3. Blood 2013; 121: 1819-23.
[70] Wan B, Zhang S, Wang P, Deng P and Dai W. Prognostic value of semi-quantitative parameters of (18)F-FDG PET/CT in newly diagnosed multiple myeloma patients. Ann Nucl Med 2023; 37: 155-65.
[71] Lee H, Hyun SH, Cho YS, Moon SH, Choi JY, Kim K and Lee KH. Semi-quantitative FDG parameters predict survival in multiple myeloma patients without autologous stem cell transplantation. Cancer Imaging 2023; 23: 104.
[72] Fonti R, Larobina M, Del Vecchio S, De Luca S, Fabbricini R, Catalano L, Pane F, Salvatore M and Pace L. Metabolic tumor volume assessed by 18F-FDG PET/CT for the prediction of outcome in patients with multiple myeloma. J Nucl Med 2012; 53: 1829-35.
[73] McDonald JE, Kessler MM, Gardner MW, Buros AF, Ntambi JA, Waheed S, van Rhee F, Zangari M, Heuck CJ, Petty N, Schinke C, Thanendrarajan S, Mitchell A, Hoering A, Barlogie B, Morgan GJ and Davies FE. Assessment of total lesion glycolysis by (18)F FDG PET/CT significantly improves prognostic value of GEP and ISS in myeloma. Clin Cancer Res 2017; 23: 1981-7.
[74] Terao T, Machida Y, Tsushima T, Miura D, Narita K, Kitadate A, Takeuchi M and Matsue K. Pre-treatment metabolic tumour volume and total lesion glycolysis are superior to conventional positron-emission tomography/computed tomography variables for outcome prediction in patients with newly diagnosed multiple myeloma in clinical practice. Br J Haematol 2020; 191: 223-30.
[75] Takahashi MES, Mosci C, Duarte GO, Pericole FV, Metze K, Lorand-Metze IGH and Ramos CD. Intensity of bone involvement: a quantitative 18F-FDG PET/CT evaluation for monitoring outcome of multiple myeloma. Nucl Med Commun 2021; 42: 1375-81.
[76] Takahashi MES, Mosci C, Souza EM, Brunetto SQ, Etchebehere E, Santos AO, Camacho MR, Miranda E, Lima MCL, Amorim BJ, de Souza C, Pericole FV, Lorand-Metze I and Ramos CD. Proposal for a quantitative (18)F-FDG PET/CT metabolic parameter to assess the intensity of bone involvement in multiple myeloma. Sci Rep 2019; 9: 16429.
[77] Wu F, Bernard S, Fayad LM, Ilaslan H, Messiou C, Moulopoulos LA and Mulligan ME. Updates and ongoing challenges in imaging of multiple myeloma: AJR expert panel narrative review. AJR Am J Roentgenol 2021; 217: 775-85.
[78] Longhitano A, Alipour R, Khot A, Bajel A, Antippa P, Slavin M and Thursky K. The role of 18F-fluorodeoxyglucose positron emission tomography/computed tomography (FDG PET/CT) in assessment of complex invasive fungal disease and opportunistic co-infections in patients with acute leukemia prior to allogeneic hematopoietic cell transplant. Transpl Infect Dis 2021; 23: e13547.
[79] Gillies RJ, Kinahan PE and Hricak H. Radiomics: images are more than pictures, they are data. Radiology 2016; 278: 563-77.

[80] Lambin P, Leijenaar RTH, Deist TM, Peerlings J, de Jong EEC, van Timmeren J, Sanduleanu S, Larue RTHM, Even AJG, Jochems A, van Wijk Y, Woodruff H, van Soest J, Lustberg T, Roelofs E, van Elmpt W, Dekker A, Mottaghy FM, Wildberger JE and Walsh S. Radiomics: the bridge between medical imaging and personalized medicine. Nat Rev Clin Oncol 2017; 14: 749-62.

[81] Yip SS and Aerts HJ. Applications and limitations of radiomics. Phys Med Biol 2016; 61: R150-66.

[82] Yu KH, Beam AL and Kohane IS. Artificial intelligence in healthcare. Nat Biomed Eng 2018; 2: 719-31.

[83] Tekkeşin A. Artificial intelligence in healthcare: past, present and future. Anatol J Cardiol 2019; 22 Suppl 2: 8-9.

[84] Allegra A, Tonacci A, Sciaccotta R, Genovese S, Musolino C, Pioggia G and Gangemi S. Machine learning and deep learning applications in multiple myeloma diagnosis, prognosis, and treatment selection. Cancers (Basel) 2022; 14: 606.

[85] Lakhani P, Prater AB, Hutson RK, Andriole KP, Dreyer KJ, Morey J, Prevedello LM, Clark TJ, Geis JR, Itri JN and Hawkins CM. Machine learning in radiology: applications beyond image interpretation. J Am Coll Radiol 2018; 15: 350-9.

[86] Trägårdh E, Borrelli P, Kaboteh R, Gillberg T, Ulén J, Enqvist O and Edenbrandt L. RECOMIA-a cloud-based platform for artificial intelligence research in nuclear medicine and radiology. EJNMMI Phys 2020; 7: 51.

[87] Sachpekidis C, Enqvist O, Ulén J, Kopp-Schneider A, Pan L, Jauch A, Hajiyianni M, John L, Weinhold N, Sauer S, Goldschmidt H, Edenbrandt L and Dimitrakopoulou-Strauss A. Application of an artificial intelligence-based tool in [(18)F] FDG PET/CT for the assessment of bone marrow involvement in multiple myeloma. Eur J Nucl Med Mol Imaging 2023; 50: 3697-708.

[88] Wang J, Shi X, Yao X, Ren J and Du X. Deep learning-based CT imaging in diagnosing myeloma and its prognosis evaluation. J Healthc Eng 2021; 2021: 5436793.

[89] Nandakumar B, Baffour F, Abdallah NH, Kumar SK, Dispenzieri A, Buadi FK, Dingli D, Lacy MQ, Hayman SR, Kapoor P, Leung N, Fonder A, Hobbs M, Hwa YL, Muchtar E, Warsame R, Kourelis TV, Go RS, Kyle RA, Gertz MA, Rajkumar SV, Klug J, Korfiatis P and Gonsalves WI. Sarcopenia identified by computed tomography imaging using a deep learning-based segmentation approach impacts survival in patients with newly diagnosed multiple myeloma. Cancer 2023; 129: 385-92.

[90] Xiong X, Wang J, Hu S, Dai Y, Zhang Y and Hu C. Differentiating between multiple myeloma and metastasis subtypes of lumbar vertebra lesions using machine learning-based radiomics. Front Oncol 2021; 11: 601699.

[91] Xiong X, Zhu Q, Zhou Z, Qian X, Hong R, Dai Y and Hu C. Discriminating minimal residual disease status in multiple myeloma based on MRI: utility of radiomics and comparison of machine-learning methods. Clin Radiol 2023; 78: e839-e846.

[92] Mesguich C, Hindie E, de Senneville BD, Tlili G, Pinaquy JB, Marit G and Saut O. Improved 18-FDG PET/CT diagnosis of multiple myeloma diffuse disease by radiomics analysis. Nucl Med Commun 2021; 42: 1135-43.

[93] Xu L, Tetteh G, Lipkova J, Zhao Y, Li H, Christ P, Piraud M, Buck A, Shi K and Menze BH. Automated whole-body bone lesion detection for multiple myeloma on (68)Ga-pentixafor PET/CT imaging using deep learning methods. Contrast Media Mol Imaging 2018; 2018: 2391925.

[94] Montesinos-López OA, Montesinos-López A, Pérez-Rodríguez P, Barrón-López JA, Martini JWR, Fajardo-Flores SB, Gaytan-Lugo LS, Santana-Mancilla PC and Crossa J. A review of deep learning applications for genomic selection. BMC Genomics 2021; 22: 19.

[95] Li K, Zhang R and Cai W. Deep learning convolutional neural network (DLCNN): unleashing the potential of (18)F-FDG PET/CT in lymphoma. Am J Nucl Med Mol Imaging 2021; 11: 327-31.

[96] Zhou Z, Jain P, Lu Y, Macapinlac H, Wang ML, Son JB, Pagel MD, Xu G and Ma J. Computer-aided detection of mantle cell lymphoma on (18)F-FDG PET/CT using a deep learning convolutional neural network. Am J Nucl Med Mol Imaging 2021; 11: 260-70.

[97] Tufail AB, Ma YK, Kaabar MKA, Martínez F, Junejo AR, Ullah I and Khan R. Deep learning in cancer diagnosis and prognosis prediction: a minireview on challenges, recent trends, and future directions. Comput Math Methods Med 2021; 2021: 9025470.

[98] Huber N, Anderson T, Missert A, Adkins M, Leng S, Fletcher J, McCollough C, Yu L and Glazebrook KN. Clinical evaluation of a phantom-based deep convolutional neural network for whole-body-low-dose and ultra-low-dose CT skeletal surveys. Skeletal Radiol 2022; 51: 145-51.

[99] Wennmann M, Ming W, Bauer F, Chmelik J, Klein A, Uhlenbrock C, Grözinger M, Kahl KC, Nonnenmacher T, Debic M, Hielscher T, Thierjung H, Rotkopf LT, Stanczyk N, Sauer S, Jauch A, Götz M, Kurz FT, Schlamp K, Horger M, Afat S, Besemer B, Hoffmann M, Hoffend J, Kraemer D, Graeven U, Ringelstein A, Bonekamp D, Kleesiek J, Floca RO, Hillengass J, Mai EK, Weinhold N, Weber TF, Goldschmidt H, Schlemmer HP, Maier-Hein K, Delorme S and Neher P. Prediction of bone marrow biopsy results from MRI in multiple myeloma patients using deep learning and radiomics. Invest Radiol 2023; 58: 754-65.

[100] Tagliafico AS, Piana M, Schenone D, Lai R, Massone AM and Houssami N. Overview of radiomics in breast cancer diagnosis and prognostication. Breast 2020; 49: 74-80.

[101] Park H, Lee SY, Lee J, Pak J, Lee K, Lee SE and Jung JY. Detecting multiple myeloma infiltration of the bone marrow on CT scans in patients with osteopenia: feasibility of radiomics analysis. Diagnostics (Basel) 2022; 12: 923.

[102] Schenone D, Dominietto A, Campi C, Frassoni F, Cea M, Aquino S, Angelucci E, Rossi F, Torri L, Bignotti B, Tagliafico AS and Piana M. Radiomics and artificial intelligence for outcome prediction in multiple myeloma patients undergoing autologous transplantation: a feasibility study with CT data. Diagnostics (Basel) 2021; 11: 1759.

[103] Li Y, Liu Y, Yin P, Hao C, Sun C, Chen L, Wang S and Hong N. MRI-based bone marrow radiomics nomogram for prediction of overall survival in patients with multiple myeloma. Front Oncol 2021; 11: 709813.

[104] Li Y, Yin P, Liu Y, Hao C, Chen L, Sun C, Wang S and Hong N. Radiomics models based on magnetic resonance imaging for prediction of the response to bortezomib-based therapy in patients with multiple myeloma. Biomed Res Int 2022; 2022: 6911246.

[105] Liu J, Guo W, Zeng P, Geng Y, Liu Y, Ouyang H, Lang N and Yuan H. Vertebral MRI-based radiomics model to differentiate multiple myeloma from metastases: influence of features number on logistic regression model performance. Eur Radiol 2022; 32: 572-81.

[106] Liu J, Wang C, Guo W, Zeng P, Liu Y, Lang N and Yuan H. A preliminary study using spinal MRI-based radiomics to

predict high-risk cytogenetic abnormalities in multiple myeloma. Radiol Med 2021; 126: 1226-35.
[107] Liu J, Zeng P, Guo W, Wang C, Geng Y, Lang N and Yuan H. Prediction of high-risk cytogenetic status in multiple myeloma based on magnetic resonance imaging: utility of radiomics and comparison of machine learning methods. J Magn Reson Imaging 2021; 54: 1303-11.
[108] Wennmann M, Klein A, Bauer F, Chmelik J, Grözinger M, Uhlenbrock C, Lochner J, Nonnenmacher T, Rotkopf LT, Sauer S, Hielscher T, Götz M, Floca RO, Neher P, Bonekamp D, Hillengass J, Kleesiek J, Weinhold N, Weber TF, Goldschmidt H, Delorme S, Maier-Hein K and Schlemmer HP. Combining deep learning and radiomics for automated, objective, comprehensive bone marrow characterization from whole-body MRI: a multicentric feasibility study. Invest Radiol 2022; 57: 752-63.
[109] Wennmann M, Neher P, Stanczyk N, Kahl KC, Kächele J, Weru V, Hielscher T, Grözinger M, Chmelik J, Zhang KS, Bauer F, Nonnenmacher T, Debic M, Sauer S, Rotkopf LT, Jauch A, Schlamp K, Mai EK, Weinhold N, Afat S, Horger M, Goldschmidt H, Schlemmer HP, Weber TF, Delorme S, Kurz FT and Maier-Hein K. Deep learning for automatic bone marrow apparent diffusion coefficient measurements from whole-body magnetic resonance imaging in patients with multiple myeloma: a retrospective multicenter study. Invest Radiol 2023; 58: 273-82.
[110] Wu Z, Bian T, Dong C, Duan S, Fei H, Hao D and Xu W. Spinal MRI-based radiomics analysis to predict treatment response in multiple myeloma. J Comput Assist Tomogr 2022; 46: 447-54.
[111] Wu Z, Wang H, Zheng Y, Fei H, Dong C, Wang Z, Ren W, Xu W and Bian T. Lumbar MR-based radiomics nomogram for detecting minimal residual disease in patients with multiple myeloma. Eur Radiol 2023; 33: 5594-605.
[112] Zhang S, Liu M, Li S, Cui J, Zhang G and Wang X. An MRI-based radiomics nomogram for differentiating spinal metastases from multiple myeloma. Cancer Imaging 2023; 23: 72.
[113] Jin Z, Wang Y, Wang Y, Mao Y, Zhang F and Yu J. Application of 18F-FDG PET-CT images based radiomics in identifying vertebral multiple myeloma and bone metastases. Front Med (Lausanne) 2022; 9: 874847.
[114] Ni B, Huang G, Huang H, Wang T, Han X, Shen L, Chen Y and Hou J. Machine learning model based on optimized radiomics feature from (18)F-FDG-PET/CT and clinical characteristics predicts prognosis of multiple myeloma: a preliminary study. J Clin Med 2023; 12: 2280.
[115] Zhong H, Huang D, Wu J, Chen X, Chen Y and Huang C. (18)F-FDG PET/CT based radiomics features improve prediction of prognosis: multiple machine learning algorithms and multimodality applications for multiple myeloma. BMC Med Imaging 2023; 23: 87.
[116] Papanikolaou N, Matos C and Koh DM. How to develop a meaningful radiomic signature for clinical use in oncologic patients. Cancer Imaging 2020; 20: 33.
[117] Latifoltojar A, Boyd K, Riddell A, Kaiser M and Messiou C. Characterising spatial heterogeneity of multiple myeloma in high resolution by whole body magnetic resonance imaging: towards macro-phenotype driven patient management. Magn Reson Imaging 2021; 75: 60-4.
[118] Rasche L, Chavan SS, Stephens OW, Patel PH, Tytarenko R, Ashby C, Bauer M, Stein C, Deshpande S, Wardell C, Buzder T, Molnar G, Zangari M, van Rhee F, Thanendrarajan S, Schinke C, Epstein J, Davies FE, Walker BA, Meissner T, Barlogie B, Morgan GJ and Weinhold N. Spatial genomic heterogeneity in multiple myeloma revealed by multi-region sequencing. Nat Commun 2017; 8: 268.
[119] Scapicchio C, Gabelloni M, Barucci A, Cioni D, Saba L and Neri E. A deep look into radiomics. Radiol Med 2021; 126: 1296-311.
[120] Wennmann M and Murray JM. Potential of radiomics and artificial intelligence in myeloma imaging: development of automatic, comprehensive, objective skeletal analyses from whole-body imaging data. Radiologe 2022; 62: 44-50.
[121] Keskinbora KH. Medical ethics considerations on artificial intelligence. J Clin Neurosci 2019; 64: 277-82.
[122] Randhawa GK and Jackson M. The role of artificial intelligence in learning and professional development for healthcare professionals. Healthc Manage Forum 2020; 33: 19-24.
[123] Almeida SD, Santinha J, Oliveira FPM, Ip J, Lisitskaya M, Lourenço J, Uysal A, Matos C, João C and Papanikolaou N. Quantification of tumor burden in multiple myeloma by atlas-based semi-automatic segmentation of WB-DWI. Cancer Imaging 2020; 20: 6.
[124] Klein A, Warszawski J, Hillengaß J and Maier-Hein KH. Automatic bone segmentation in whole-body CT images. Int J Comput Assist Radiol Surg 2019; 14: 21-9.
[125] Muchtar E, Dispenzieri A, Gertz MA, Kumar SK, Buadi FK, Leung N, Lacy MQ, Dingli D, Ailawadhi S, Bergsagel PL, Fonseca R, Hayman SR, Kapoor P, Grogan M, Abou Ezzeddine OF, Rosenthal JL, Mauermann M, Siddiqui M, Gonsalves WI, Kourelis TV, Larsen JT, Reeder CB, Warsame R, Go RS, Murray DL, McPhail ED, Dasari S, Jevremovic D, Kyle RA, Lin Y, Lust JA, Russell SJ, Hwa YL, Fonder AL, Hobbs MA, Rajkumar SV, Roy V and Sher T. Treatment of AL amyloidosis: mayo stratification of myeloma and risk-adapted therapy (mSMART) consensus statement 2020 update. Mayo Clin Proc 2021; 96: 1546-77.
[126] Palumbo A, Bringhen S, Mateos MV, Larocca A, Facon T, Kumar SK, Offidani M, McCarthy P, Evangelista A, Lonial S, Zweegman S, Musto P, Terpos E, Belch A, Hajek R, Ludwig H, Stewart AK, Moreau P, Anderson K, Einsele H, Durie BG, Dimopoulos MA, Landgren O, San Miguel JF, Richardson P, Sonneveld P and Rajkumar SV. Geriatric assessment predicts survival and toxicities in elderly myeloma patients: an international myeloma working group report. Blood 2015; 125: 2068-74.
[127] Horger M, Fritz J, Thaiss WM, Ditt H, Weisel K, Haap M and Kloth C. Comparison of qualitative and quantitative CT and MRI parameters for monitoring of longitudinal spine involvement in patients with multiple myeloma. Skeletal Radiol 2018; 47: 351-61.
[128] Koutoulidis V, Terpos E, Klapa I, Cheliotis G, Ntanasis-Stathopoulos I, Boultadaki A, Gavriatopoulou M, Kastritis E, Dimopoulos MA and Moulopoulos LA. Whole-body low-dose CT in multiple myeloma: diagnostic value of appendicular medullary patterns of attenuation. AJR Am J Roentgenol 2021; 216: 742-51.
[129] Maggialetti N, Ferrari C, Nappi AG, Quinto A, Rossini B, Zappia M, Minoia C, Guarini A, Brunese L and Rubini G. Is whole body low dose CT still necessary in the era of (18) F-FDG PET/CT for the assessment of bone disease in multiple myeloma patients? Hell J Nucl Med 2020; 23: 264-71.
[130] Simeone FJ, Harvey JP, Yee AJ, O'Donnell EK, Raje NS, Torriani M and Bredella MA. Value of low-dose whole-body CT

in the management of patients with multiple myeloma and precursor states. Skeletal Radiol 2019; 48: 773-9.
[131] Hu C, Zhang Y, Xiong X, Meng Q, Yao F, Ye A and Hao Z. Quantitative evaluation of bone marrow infiltration using dual-energy spectral computed tomography in patients with multiple myeloma. J Xray Sci Technol 2021; 29: 463-75.
[132] Winkelmann MT, Hagen F, Le-Yannou L, Weiss J, Riffel P, Gutjahr R, Faby S, Nikolaou K and Horger M. Myeloma bone disease imaging on a 1st-generation clinical photon-counting detector CT vs. 2nd-generation dual-source dual-energy CT. Eur Radiol 2023; 33: 2415-25.
[133] Koutoulidis V, Fontara S, Terpos E, Zagouri F, Matsaridis D, Christoulas D, Panourgias E, Kastritis E, Dimopoulos MA and Moulopoulos LA. Quantitative diffusion-weighted imaging of the bone marrow: an adjunct tool for the diagnosis of a diffuse MR imaging pattern in patients with multiple myeloma. Radiology 2017; 282: 484-93.
[134] Zhou C, Chan HP, Dong Q, Couriel DR, Pawarode A, Hadjiiski LM and Wei J. Quantitative analysis of MR imaging to assess treatment response for patients with multiple myeloma by using dynamic intensity entropy transformation: a preliminary study. Radiology 2016; 278: 449-57.
[135] ElGendy K, Barwick TD, Auner HW, Chaidos A, Wallitt K, Sergot A and Rockall A. Repeatability and test-retest reproducibility of mean apparent diffusion coefficient measurements of focal and diffuse disease in relapsed multiple myeloma at 3T whole body diffusion-weighted MRI (WB-DW-MRI). Br J Radiol 2022; 95: 20220418.
[136] Takahashi MES, Mosci C, Souza EM, Brunetto SQ, de Souza C, Pericole FV, Lorand-Metze I and Ramos CD. Computed tomography-based skeletal segmentation for quantitative PET metrics of bone involvement in multiple myeloma. Nucl Med Commun 2020; 41: 377-82.
[137] Stolzenburg A, Lückerath K, Samnick S, Speer M, Kneer K, Schmid JS, Grigoleit GU, Hofmann S, Beer AJ, Bunjes D, Knop S, Buck AK, Einsele H and Lapa C. Prognostic value of [(18)F]FDG-PET/CT in multiple myeloma patients before and after allogeneic hematopoietic cell transplantation. Eur J Nucl Med Mol Imaging 2018; 45: 1694-704.
[138] Sachpekidis C, Merz M, Kopp-Schneider A, Jauch A, Raab MS, Sauer S, Hillengass J, Goldschmidt H and Dimitrakopoulou-Strauss A. Quantitative dynamic (18)F-fluorodeoxyglucose positron emission tomography/computed tomography before autologous stem cell transplantation predicts survival in multiple myeloma. Haematologica 2019; 104: e420-e423.
[139] Faghani S, Baffour FI, Ringler MD, Hamilton-Cave M, Rouzrokh P, Moassefi M, Khosravi B and Erickson BJ. A deep learning algorithm for detecting lytic bone lesions of multiple myeloma on CT. Skeletal Radiol 2023; 52: 91-8.
[140] Gong H, Baffour FI, Glazebrook KN, Rhodes NG, Tiegs-Heiden CA, Thorne JE, Cook JM, Kumar S, Fletcher JG, McCollough CH and Leng S. Deep learning-based virtual non-calcium imaging in multiple myeloma using dual-energy CT. Med Phys 2022; 49: 6346-58.
[141] Bao L, Wang YT, Zhuang JL, Liu AJ, Dong YJ, Chu B, Chen XH, Lu MQ, Shi L, Gao S, Fang LJ, Xiang QQ and Ding YH. Machine learning-based overall survival prediction of elderly patients with multiple myeloma from multicentre real-life data. Front Oncol 2022; 12: 922039.
[142] Yan W, Shi H, He T, Chen J, Wang C, Liao A, Yang W and Wang H. Employment of artificial intelligence based on routine laboratory results for the early diagnosis of multiple myeloma. Front Oncol 2021; 11: 608191.
[143] Morvan L, Carlier T, Jamet B, Bailly C, Bodet-Milin C, Moreau P, Kraeber-Bodéré F and Mateus D. Leveraging RSF and PET images for prognosis of multiple myeloma at diagnosis. Int J Comput Assist Radiol Surg 2020; 15: 129-39.